Mineralium Deposita (2025) 60:237–259
https://doi.org/10.1007/s00126-024-01278-z

ARTICLE

Melt infiltration in a crystal mush and pegmatoid formation in the platiniferous Merensky Reef, Bushveld Complex, South Africa

Ben Hayes[1] · Reza Maghdour-Mashhour[1,2] · Lewis D. Ashwal[1] · Albertus J.B. Smith[3,4] · Henriette Ueckermann[3] · Jaco Vermeulen[5]

Received: 4 April 2024 / Accepted: 30 April 2024 / Published online: 27 May 2024

Abstract

Giant mafic-ultramafic layered intrusions of Archaean-Proterozoic age are the fossilised remnants of huge injections of silicate magma in the Earth's crust and are our most important repositories of platinum-group elements. Magmatic PGE-rich ore deposits, such as the Merensky Reef, are typically hosted in stratiform reefs at the contacts between ultramafic and feldspathic cumulates. The Merensky Reef is commonly characterised by coarse-grained and pegmatoidal textures that may provide important clues to its origin. We present textural and in situ geochemical data for Merensky pegmatoids at Styldrift Mine (Impala Bafokeng) in the Western Bushveld Complex of South Africa. This region is adjacent to an inferred magmatic feeder zone to the Bushveld. The Merensky pegmatoids are characterised by (i) amoeboid olivine inclusions in zoned orthopyroxene megacrysts with increasing molar Mg# of orthopyroxene towards olivine, (ii) fine-grained chains of orthopyroxene in compositional equilibrium with adjacent orthopyroxene megacrysts, (iii) increasing molar Mg# of orthopyroxene megacrysts and increasing molar An with decreasing $^{87}Sr/^{86}Sr_i$ (at 2.06 Ga) of plagioclase oikocrysts in pegmatoids laterally across a 10-km section distal to the feeder, and (iv) highly variable molar An and initial $^{87}Sr/^{86}Sr_i$ of interstitial plagioclase proximal to the feeder. We interpret the coarse-grained and pegmatoidal textures, their dissolution-reprecipitation features, and lateral chemical variations as the product of lateral melt infiltration and mixing in a crystal mush. We suggest that the platiniferous Merensky Reef was not formed at the base of a large melt-filled magma chamber but was instead the product of non-sequential magma emplacement that rejuvenated the crystal mush.

Keywords Bushveld Complex · Merensky Reef · Crystal mush · Melt infiltration · PGE mineralisation

Introduction

The Rustenburg Layered Suite (RLS) of the Bushveld Complex in South Africa is the fossilised remnant of a giant Paleoproterozoic basaltic magma chamber that hosts the largest resources of platinum-group elements (PGE), chromium, and vanadium on the planet. One of the most well-known PGE ore bodies is the Merensky Reef which was first discovered in 1924 (Cawthorn 1999a). The petrogenesis of the Merensky Reef has been a topic of debate for many decades and understanding its origin requires a nuanced understanding of the magmatic processes that operated to produce the first-order macro rhythmic igneous layering in the RLS. One group of researchers have proposed that the Merensky Reef was formed at the base of a large melt-filled chamber (e.g., Campbell et al. 1983; Cawthorn and Boerst 2006; Naldrett et al. 2009; Latypov et al. 2017; Latypov et al. 2022). However, another group has challenged this

Editorial handling: E. Mansur.

✉ Ben Hayes
ben.hayes@wits.ac.za

[1] School of Geosciences, University of the Witwatersrand, Johannesburg 2050, South Africa

[2] Department of Earth Sciences, Carleton University, 2115 Herzberg Laboratories, Ottawa, ON K1S 5B6, Canada

[3] Paleoproterozoic Mineralisation Research (PPM), Department of Geology, University of Johannesburg, Johannesburg 2006, South Africa

[4] Department of Science and Innovation-National Research Foundation Centre of Excellence in Mineral and Energy Resource Analysis, Department of Geology, University of Johannesburg, Johannesburg 2006, South Africa

[5] Impala Bafokeng Limited, 2 Fricker Road, Illovo, Johannesburg 2196, South Africa

concept of igneous layering, and the associated stratiform ore bodies, forming at the base of a large melt-filled chamber by multiple lines of textural, geochemical, and geochronological evidence from the RLS (e.g., Mungall et al. 2016; Hayes et al. 2018; Mitchell et al. 2019; Scoates et al. 2021; Maghdour-Mashhour et al. 2021; Yao et al. 2021). This questions the notion that the Merensky Reef is the product of a large melt-filled chamber.

The Merensky Reef is a remarkably laterally extensive stratiform layer of PGE-enriched feldspathic pyroxenite in the Upper Critical Zone of the RLS and is typically bracketed by thin (~1 cm) lower and upper chromite stringers. The Merensky Reef has been described as an irregular regional unconformity in the RLS and is unequivocally associated with the injection of new magma into the crystallising chamber (Viljoen 1999; Kruger 2005; Cawthorn 2015). The evidence for magma replenishment is compelling and includes potholes representing magmatic erosion features that transgress into the underlying anorthositic footwall rocks (e.g., Viljoen 1999; Latypov et al. 2015) and a major shift in the bulk rock $^{87}Sr/^{86}Sr$ isotopic composition of the cumulate rocks at the level of the Merensky Reef (Kruger, 1992 Kruger 2005). The question is whether magma replenishment was a basal flow in a large melt-filled chamber or a "sill-like" injection of magma into a partly solidified or mushy chamber.

The Merensky Reef is mostly medium (1–5 mm) to coarse-grained (5–30 mm) in texture but is locally pegmatoidal (> 30 mm). The origin of the pegmatoids has previously been explained by the recrystallisation of cumulate material by slow cooling induced by an overlying hot magma (e.g., Campbell et al. 1983; Viljoen 1999; Cawthorn and Boerst 2006), or volatile-induced crystal growth (e.g., Vermaak 1976; Nicholson and Mathez 1991). Some have speculated that the pegmatoid-forming process also produced high PGE tenors (e.g., Irvine et al. 1983; Viljoen et al. 1986; Viljoen 1999; Boudreau 2008; Prevec et al. 2021). Therefore, understanding the origin of the pegmatoids may be the key to understanding the origin of the PGE mineralisation.

In this study, we investigate the textures and mineral compositions of Merensky pyroxenites and pegmatoids in a 10 km section of the Upper Critical Zone at Styldrift Mine (Impala Bafokeng) in the Western Limb of the Bushveld Complex. Our findings show that the Merensky pegmatoids may have formed by the infiltration of silicate melt into a crystal mush. This has implications for the morphology of the magma chamber during Merensky Reef times and we suggest that this magmatic process could explain the origin of its high PGE metal tenors.

Geological setting

Bushveld Complex

The Paleoproterozoic Bushveld Complex was emplaced onto the Kaapvaal craton at 2.06 Ga (e.g., Zeh et al. 2015; Mungall et al. 2016; Scoates et al. 2021). The Complex is divided into four major components: (1) the Rooiberg Group, a suite of mafic and felsic lavas; (2) the RLS, a 6–8 km thick sequence of layered mafic-ultramafic cumulates; (3) the Rashoop Granophyre, a thin (< 1 km) granitic layer at the top of the RLS; and (4) the Lebowa Granite Suite, a 1–2 km thick sequence of K-feldspar-bearing granites that represent the products of large-scale crustal melting during emplacement of mantle-derived magmas into the RLS (Cawthorn 2015). The relatively short duration (< 5 Myr) and large volume (> 1 Mkm^3) of magmatism qualify the Bushveld Complex as a large igneous province (Ernst 2014).

In the most general sense, the RLS preserves a differentiated sequence of igneous rocks from orthopyroxenites at the base to ferrogabbros and ferrodiorites at the top. At the base is the Lower Zone, which is distributed in a series of compartments in the Eastern and Western Limbs (Fig. 1). The Lower Zone is characterised mostly by orthopyroxenites with localised olivine-bearing layers of harzburgite and dunite (Cameron 1980). A stratigraphically deeper extension of Lower Zone cumulates with locally developed komatiitic chill margins, known as the Basal Ultramafic Sequence, has been identified in parts of the Eastern Limb (Wilson et al. 2012), which may also be part of a 'Marginal Phase' (Scoon and Mitchell 2023). The Basal Ultramafic Sequence and Lower Zone are divided by a thin and discontinuous package of fine- to medium-grained poorly layered gabbronorites known as the Marginal Zone, possibly representing chilled and/or parental magmas (Harmer and Sharpe, 1985). The Lower Zone grades into orthopyroxenites of the Lower Critical Zone with the content of interstitial plagioclase increasing and thick (up to 1 m) chromitite layers developed (e.g., Lower Group and Middle Group chromitites: Cameron 1980). The Upper Critical Zone starts at the Middle Group-3 chromitite (Cameron 1980; Maghdour-Mashhour et al. 2021) and is mostly characterised by alternating layers of chromitite, pyroxenite and feldspathic cumulates (i.e., norites and anorthosites). The feldspathic cumulates are typically poikilitic in texture with discontinuous layering partly defined by the alignment of orthopyroxene oikocrysts with complex plagioclase schlieren. The Upper Critical Zone is economically significant as it contains the PGE-enriched UG-2 chromitite and Merensky Reef, both of which are extraordinarily laterally extensive ore bodies over distances of hundreds of km. High-precision U-Pb dating of zircon

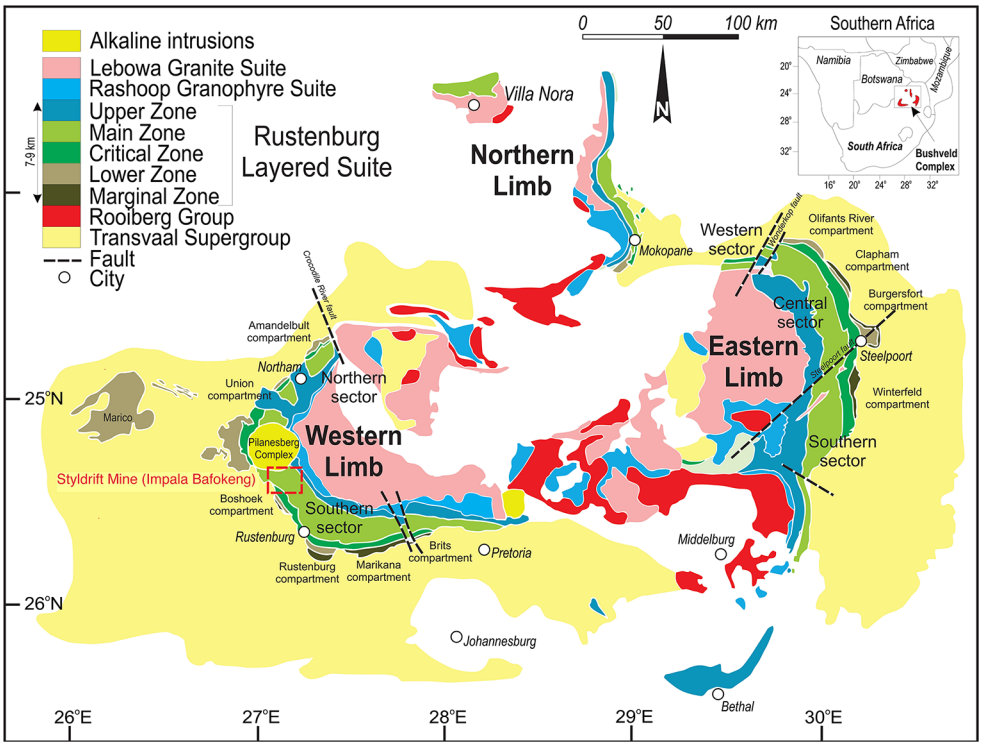

Fig. 1 A simplified geological map of the Bushveld Complex. (modified from Yao et al. 2021). The red dashed box outlines the location of Styldrift Mine (Impala Bafokeng) in the southern sector of the Western Limb

shows that the Merensky Unit has indistinguishable ages in both the Eastern (2056.88 ± 0.41 Ma) and Western Limbs (2057.04 ± 0.55 Ma) (Scoates and Wall 2015). The Platreef (and Flatreef) are the PGE-rich ore body equivalents in the Northern Limb of the Bushveld Complex (Kinnaird 2005; Grobler et al. 2019). There is also the enigmatic Waterberg Project to the north of the Hout River Shear Zone with its F- and T-Zones associated with Lower Zone-type material and Main Zone-type material, respectively (Kinnaird, 2017). The Upper Critical Zone is overlain by the Main Zone, a sequence of poorly layered gabbronorites with localised anorthosite and pyroxenite layering (e.g., Nex et al. 2002; Hayes et al. 2017; Bourdeau et al. 2022). Near the top of the Main Zone is a laterally extensive pyroxenite layer called the Pyroxenite Marker that represents a major (and final) voluminous input of magma into the chamber (Cawthorn et al. 1991; Setera and VanTongeren 2018; Bourdeau et al. 2023). Above the Pyroxenite Marker is the Upper Zone which consists of ferrogabbronorites with local magnetitites and ferrodiorites, containing huge resources of vanadium (Cawthorn 2015).

Merensky Reef

The term Merensky Reef has been used loosely in published literature and here we subscribe to the nomenclature defined in Cawthorn and Boerst (2006). That is, the Merensky Reef is strictly the economically PGE mineralised zone at or near the base of the Merensky Unit. The Merensky Unit can be considered as a macro-rhythmic package of rocks comprising a lower chromitite stringer, a pyroxenite (with localised pegmatoidal textures), an upper chromitite stringer, and overlying norites grading into anorthosite (i.e., the footwall to the next macro-rhythmic unit known as the Bastard Unit). It should be stressed that this is a generalised vertical section across the Merensky Unit and that there are many local variations across the entire Bushveld Complex (e.g., Viljoen 1999; Cawthorn and Boerst 2006; Mitchell and Scoon 2007; Smith et al. 2013; Latypov et al. 2015). Significant PGE mineralisation can also continue into the anorthosite to leuconorite footwall directly underlying the Merensky Unit (e.g., Smith et al. 2013).

The feldspathic pyroxenites of the Merensky Reef are typically medium (1–5 mm) to coarse-grained (5–30 mm) which we name "normal pyroxenite" henceforth (Cawthorn and Boerst 2006; Naldrett et al. (2009). Pegmatoid textures (i.e., grain sizes > 30 mm as per the IUGS classification) are common in the Merensky Reef and have been documented in many studies across the entire Bushveld Complex. We note that Cawthorn and Boerst (2006) used their own classification schemes for the Merensky pyroxenite (grain sizes < 2 mm) and Merensky pegmatoid (grain sizes > 2 mm), which we avoid here. Stratiform pegmatoids generally have the same modal abundances of orthopyroxene and plagioclase as the "normal" pyroxenite but are commonly more olivine and chromite-rich compared to the normal pyroxenite (e.g., Cawthorn and Boerst 2006). The pegmatoids may form a continuous layer at the base of the

Merensky Unit, form a discontinuous lens-like network, or be present in the upper parts of the normal Merensky pyroxenite. The pegmatoid is commonly bounded by thin (~ 1 cm) lower and upper chromitite stringers, although these chromitites are thicker where they fill pothole structures. Some have remarked that there is a close association between the PGE mineralisation and the spatial distribution of the pegmatoids (e.g., Viljoen 1999; Prevec et al. 2021) that suggests they may be a close genetic connection.

Styldrift Mine (Impala Bafokeng)

The location of Styldrift Mine (Impala Bafokeng) is significant because it is near the transition between two distinct lithofacies subtypes of the Merensky Reef, known as Swartklip and Rustenburg facies, as described below. The transition was first defined by Wagner (1929) and is largely hidden by the Pilanesberg Complex. Swartklip facies is to the north and the Rustenburg facies is to the south of the Pilanesberg Complex. The main reasons for the regional facies transition are the varying thickness of cumulate material between the UG-2 Chromitite and Merensky Reef, the more regular presence of olivine-bearing cumulates in the Swartklip facies, the regularity and sizes of potholes and the degree of textural/facies variation in the Merensky Reef itself (Viljoen 1999). Furthermore, the location of Styldrift Mine is interesting because it may coincide with a major magma feeder area to the RLS. This interpretation is supported by the high Pt tenors and low Cu/Pd observed in this region, both decreasing towards the south (Naldrett et al. 2009). There is also a significant gravity anomaly in the region (Viljoen 1999) as well as a pre-existing weakness as shown by the intrusion of the Mesoproterozoic Pilanesberg Complex ~ 600 million years later (Elburg and Cawthorn 2017).

There are significant lithofacies variations in the Merensky Unit at Styldrift Mine (Impala Bafokeng) that were summarised in detail by Moodley (2008) and Vermeulen (2010). Reef types are generally classified on the basis of marked differences in the physical nature of the reef, changes in the lithology and thickness of the footwall sequence, and the style of mineralisation (Vermeulen 2010). The names given to the different facies are as follows, from east to west on Styldrift farm: Main Reef, Normal Thick Reef, Normal Reef, Transition Reef, Central Reef, Terrace Reef, and Abutment Reef (Vermeulen 2010). We sampled from the Central Reef, Normal Reef, Normal Thick Reef, and Main Reef as shown in Fig. 2. The footwall (FW) nomenclature shown in Fig. 2 is after that developed by Leeb-du Toit (1986).

Methods

Thirty-one samples of pristine drillcore material were collected from the study area from 4 drill holes at Styldrift Mine (Impala Bafokeng) (Fig. 2). Samples were selected at regularly spaced intervals to generate a representative and detailed geochemical profile of the Upper Critical Zone, in particular the dichotomy of pyroxenites and feldspathic cumulates. Six of the 31 samples were pegmatoids.

Thirty-one thin sections were analysed quantitatively using a Cameca SX-100 electron microprobe at the Central Analytical Facility of the Faculty of Science at the University of Johannesburg (Spectrum) and ~ 1000 spot analyses of the cores and rims of grains were generated. We measured the in situ mineral chemistry of the cores of olivine ($n = 47$), orthopyroxene ($n = 168$), plagioclase ($n = 221$) and clinopyroxene ($n = 39$) both along dip and across the stratigraphy for all four drill cores and these data give the best indications of the primary magmatic composition. The operating conditions were a 15 kV accelerating potential and a 10–20 nA current. The following standards were used for Ka X-ray line calibration of minerals: diopside for Si, wollastonite for Ca, rutile for Ti, corundum for Al, hematite for Fe, rhodonite for Mn, periclase for Mg, jadeite for Na, orthoclase for K. The entire mineral compositional dataset is included in Appendix Table 1.

We collected $^{87}Sr/^{86}Sr$ isotope ratios for plagioclase for each pegmatoid sample, as well as for normal Merensky pyroxenite, and the footwall and hangingwall anorthosites. The $^{87}Sr/^{86}Sr$ isotopic results were collected on a ASI-Resolution 193 nm Excimer LA system connected to a Nu Plasma II Multicollector (MC)-ICP-MS at Spectrum at the University of Johannesburg following the same procedures outlined in Maghdour-Mashhour et al. (2021). A BHVO2 glass ($^{87}Sr/^{86}Sr = 0.703469 \pm 0.000014$: Elburg et al. 2005) and a virtually Rb-free in-house plagioclase glass ($^{87}Sr/^{86}Sr = 0.70719 \pm 2$ (2SD on three TIMS determinations: Elburg, personal communication) were continually measured during the session. Both reference materials reproduced the accepted values for BHVO2 with $^{87}Sr/^{86}Sr$ of 0.703462 ± 0.00027 (2SD: $n = 13$) and the in-house plagioclase standard producing an average $^{87}Sr/^{86}Sr$ of 0.707063 ± 0.00007 (2SD: $n = 6$). The Rb-Sr isotopic compositional data for the samples and standards are included in Appendix Table 2.

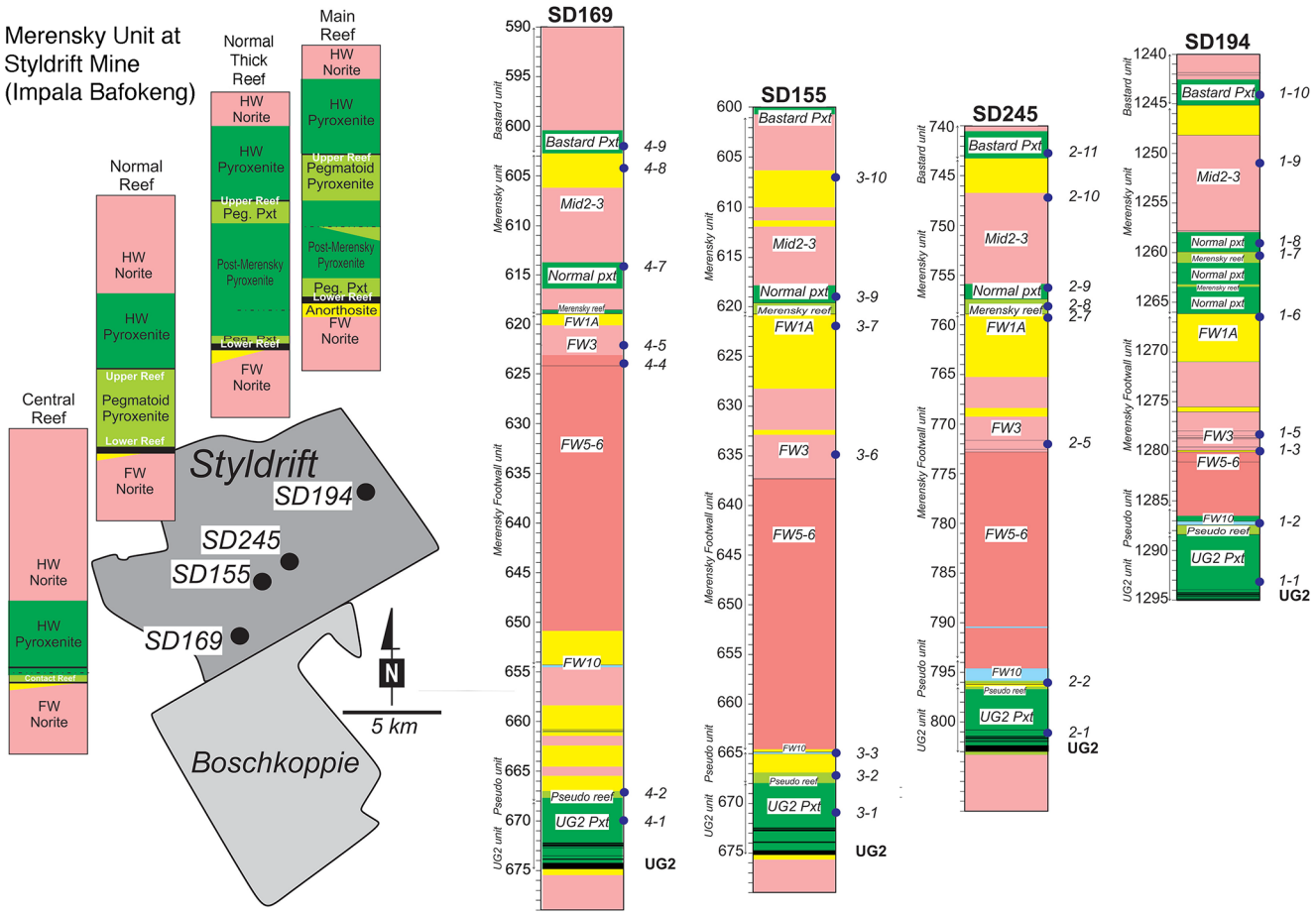

Fig. 2 The location of the drill holes (SD194, SD245, SD155, and SD169) are shown on Styldrift farm adjacent to Boschkoppie farm at Impala Bafokeng. A generalized stratigraphic column of each drillcore is shown with Main Reef (SD194), Normal Thick Reef (SD245), Normal Reef (SD155) and Contact Reef (SD169) facies types all characterised. Detailed stratigraphic logs of the drill cores between the UG-2 chromitite and the Bastard Reef are also shown along with the locations of the samples used in this study

Results

Lithofacies variations at Styldrift Mine (Impala Bafokeng)

We studied 4 vertical sections of the Upper Critical Zone from drillcores at Styldrift Mine (Impala Bafokeng) in the Western Limb of the Bushveld Complex (Fig. 1), which extend across the UG-2 Unit pyroxenite, the Merensky Unit, and the hangingwall anorthosites of the Bastard Unit. This succession includes the sub-economic Pseudoreef (colloquially known as the "Tarentaal Reef"), which occurs stratigraphically just above the UG-2 Unit.

The lithostratigraphic succession of the Merensky Unit at Styldrift Mine can be summarised as follows, from the base to the top: The lowermost rocks (footwall) consist of anorthosite and leuconorite locally exhibiting mottled and spotted textures (Fig. 3); a lower chromite stringer (Fig. 3c); a layer of pegmatoidal orthopyroxenite ranging in thickness from ~ 10 cm to 2 m (Fig. 3c, d, f); an upper chromite stringer; a layer of coarse-grained ("normal") orthopyroxenite above the pegmatoid layer (Fig. 3d); and a thick overlying (hangingwall) sequence of norite to leuconorite with distinctive mottled textures. The footwall anorthosite ranges in thickness from 0.5 to 6 m and is locally termed a "boulder bed" because of the presence of rounded inclusions of pegmatoidal pyroxenite (Moodley 2008). The footwall unit shows small (cm-m) lengthscale variations in modal abundances of plagioclase and pyroxene which have led to numerous subdivisions of the facies types (Moodley 2008). In places, the lower chromite stringer may be up to 4–5 cm thick (Fig. 3b). The pegmatoidal pyroxenite may also be patchy in its distribution (Fig. 3e). The upper chromite stringer is typically < 1 cm thick. The highest grades of PGE mineralisation occur in the vicinity of the upper chromite stringer and in the pegmatoidal facies between the upper and lower chromite stringers (e.g., Campbell et al. 1983; Prevec 2018). The vertical thickness between the chromite stringers may vary from less than 1 cm to several metres (Moodley 2008). The normal orthopyroxenite overlying the PGE-mineralised

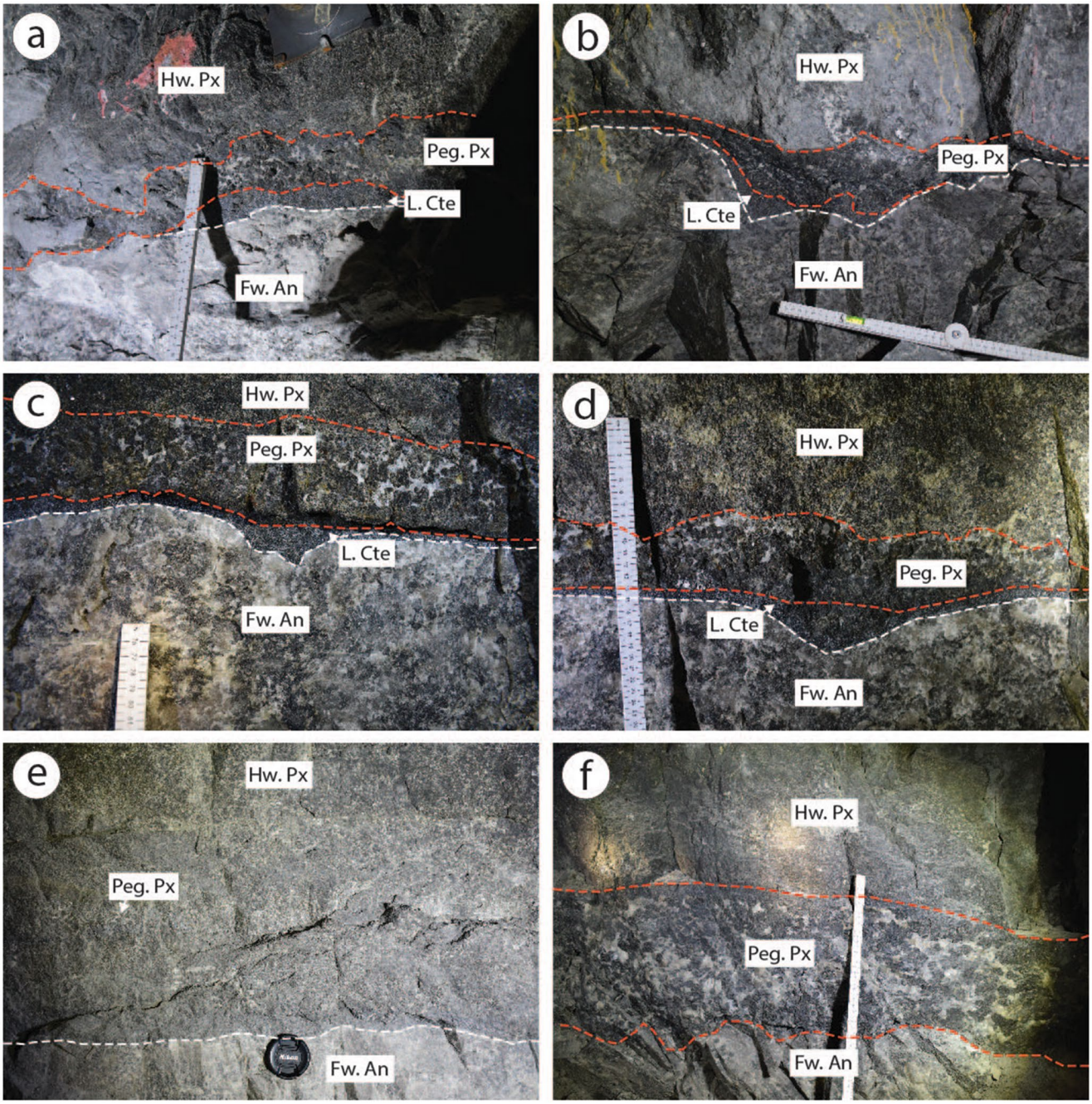

Fig. 3 Photographs of the Merensky Reef underground at Styldrift Mine (Impala Bafokeng). (**a**) Patchy and semi-layered pegmatoid (Peg. Px) in irregular contact with its hangingwall pyroxenite (Hw. Px). The lower chromitite stringer (L. Cte) is irregular in thickness and has a sharp contact with its footwall anorthosite (Fw. An). (**b**) A chromitite-filled pothole at the base of the Merensky pegmatoid (with interstitial Po-Ccp). (**c**) A thin layer of pegmatoid and a well-developed lower chromitite stringer forming a pothole. (**d**) This photo is a few metres away from (**c**) and shows the irregular upper contact of the pegmatoid with its hangingwall pyroxenite. (**e**) A more feldspar-rich variant of the Merensky pyroxenite with patchy pegmatoid textures and no lower chromitite stringer. (**f**) A well-developed pegmatoid layer in sharp contact with its hangingwall pyroxenite and a lower chromitite stringer developed on top of the footwall anorthosite

zone may be up to 10 m thick and in places a similar unit is present in the pegmatoidal pyroxenite (this was referred to as the "Pre-Merensky Pyroxenite" by Naldrett et al. 2009). The hangingwall pyroxenite sequence is typically ~ 10 m thick and grades into norite and then anorthosite which underlies the Bastard Unit.

The Pseudoreef Unit (includes Footwall 10 as shown in Fig. 2) is olivine-rich and is composed of troctolites and harzburgites with coarse-grained pegmatoidal textures, where

large subhedral or anhedral olivine grains are embedded in a matrix of interstitial plagioclase and/or orthopyroxene (as also described by Eales et al. 1988; Maier and Eales 1997; Maier et al. 2021).

The Bastard Unit overlies the Merensky Unit with both having similar lithostratigraphic sequences. It consists of a thin basal chromite layer, typically less than 5 mm thick, followed by a normal pyroxenite layer that is around 2–3 m thick. This is followed by norite and the 50-meter-thick "Giant Mottled Anorthosite" layer (Mitchell and Manthree 2002). The pyroxenites of the Bastard Unit have subeconomic quantities of PGE. Also, unlike the Merensky pyroxenite, the Bastard pyroxenite does not transgress into its footwall and is defined by a sharp contact with the underlying Merensky Unit anorthosite.

Microstructures

Typical textures in the footwall anorthosites to the Merensky Unit (FW5-6 and FW1-A) are shown in Fig. 4a-b. The footwall anorthosite contains ~ 90 vol% euhedral plagioclase laths (2–3 mm) surrounded by 10 vol% orthopyroxene and clinopyroxene oikocrysts (up to 50 mm in size).

The "normal" Merensky pyroxenites are feldspathic orthopyroxenites with adcumulate and mesocumulate textures. In general, they are made up of 60–70 vol% euhedral-subhedral orthopyroxene primocrysts (1–2 mm) surrounded

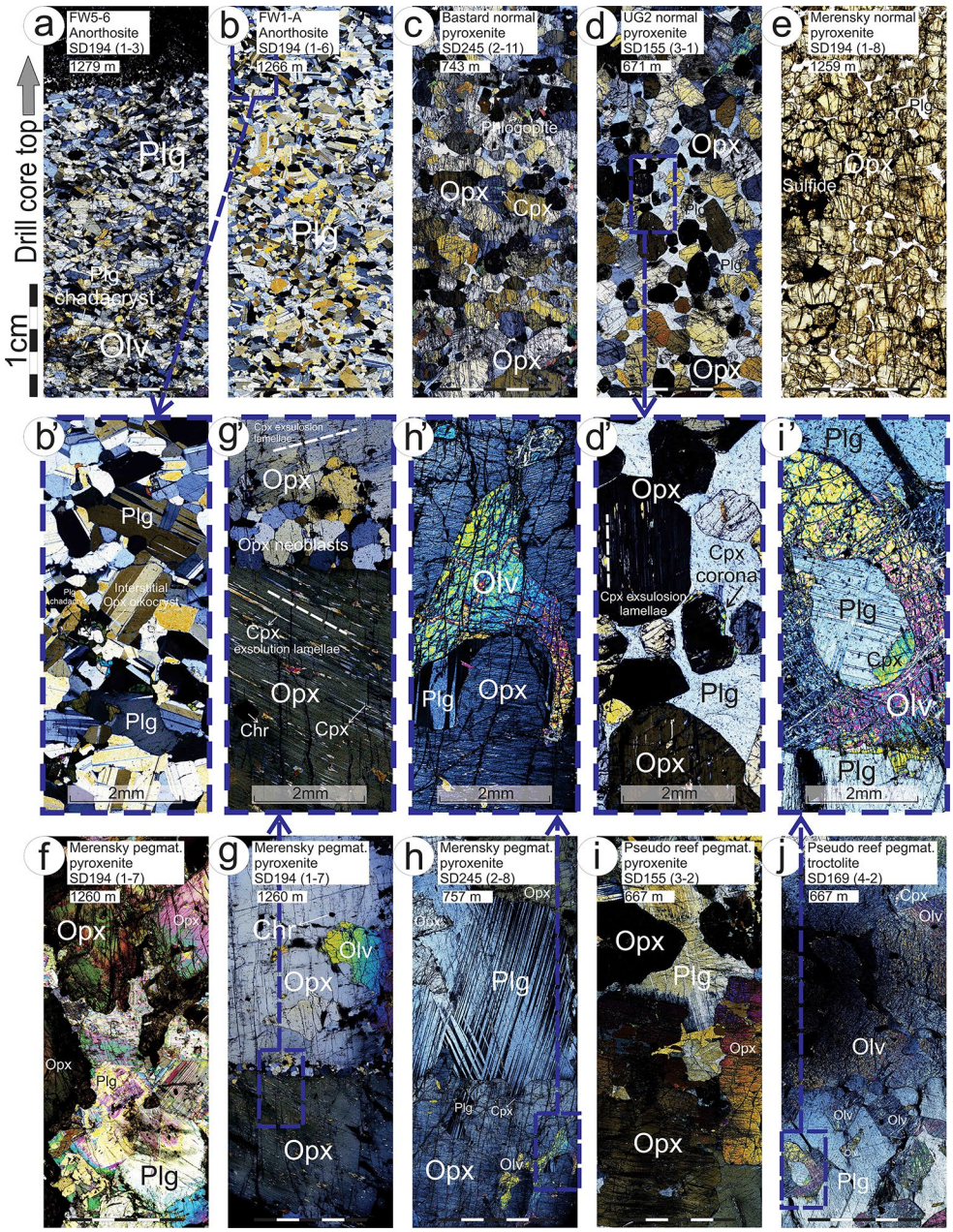

Fig. 4 Cross-polarized photomicrographs of anorthosite, normal pyroxenite and pegmatoidal pyroxenite from the UG-2 Unit to the Bastard Reef Unit. Sample depth (metres) is marked on each photomicrograph. The top of each image is towards the top of the drillcore. (**a**) FW5-6 anorthosite from SD194 (sample # 1–3) showing its contact with a chromitite stringer. (**b**) FW1-A anorthosite from SD194 (sample # 1–6) with zoom in (**b**') showing plagioclase laths and interstitial orthopyroxene oikocryst. (**c**) Normal pyroxenite of the Bastard Unit from SD245 (sample # 2–11). (**d**) Normal pyroxenite of the UG-2 Unit from SD155 (sample # 3 – 1) with zoom in (**d**') showing euhedral orthopyroxene primocrysts cemented by interstitial plagioclase. (**e**) Normal pyroxenite of the Merensky Unit from SD194 (sample # 1–8) with interstitial sulfide. (**f**, **g**) Pegmatitic pyroxenite of the Merensky Unit from SD194 (sample # 1–7) (thin section thickness > 30 microns) with zoom-in (**g**') showing a fine-grained chain of orthopyroxene neoblasts between orthopyroxene megacrysts. (**h**) Pegmatitic pyroxenite of the Merensky Unit from SD245 (sample # 2–8) with zoom in (**h**') showing amoeboid olivine inclusions in orthopyroxene. (**i**) Pegmatitic pyroxenite of the Pseudoreef from SD155 (sample # 3 – 2). (**j**) Pegmatitic pyroxenite of the Pseudoreef from SD169 (sample # 3 – 2) with zoom in (**i**') showing a plagioclase-clinopyroxene inclusion in amoeboid olivine

by interstitial plagioclase, and clinopyroxene, chromite and sulfide (Fig. 4c-e). The orthopyroxene primocrysts contain discontinuous exsolution lamellae of clinopyroxene (Fig. 4d'). There is 15–25 vol% interstitial plagioclase and 5 vol% interstitial clinopyroxene with both phases forming oikocrysts up to several centimetres in size. Clinopyroxene also locally rims orthopyroxene (Fig. 4d'). The feldspathic orthopyroxenites contain up to 5 vol% sulfide and < 2 vol% chromite, and minor (typically < 3 vol%) phlogopite and amphibole (Fig. 4c-e). Rare chromite grains (< 1 mm) are disseminated and are hosted in orthopyroxene primocrysts and interstitial plagioclase oikocrysts. The sulfides form interstitial phases between the orthopyroxene primocrysts and are present throughout the "normal" pyroxenites (Fig. 4e).

The pegmatoidal feldspathic orthopyroxenite typically comprises megacrystic orthopyroxene primocrysts (> 5 mm) cemented by interstitial plagioclase and clinopyroxene oikocrysts with modal abundances comparable to the "normal" pyroxenites (Fig. 4f-j). Olivine is also present (4 vol%) as oikocrysts (Fig. 4j) and as amoeboid inclusions in orthopyroxene (Fig. 4g), along with minor chromite (3 vol%), and sulfide (3 vol%). Chromite and sulfide are typically present as inclusions in the orthopyroxene megacrysts (Fig. 4g). The orthopyroxene megacrysts are also commonly surrounded by finer-grained orthopyroxene (Fig. 4g').

Mineral compositions

The mineral compositional data for our samples both upsection and laterally (along dip) are shown in Figs. 5, 6, 7, 8 and 9. Figure 5 shows molar Mg# (Mg# = atomic Mg/(Mg + Fe + Mn) x 100) of orthopyroxene and Fo (Fo = atomic Mg/(Mg + Fe + Mn) x 100) of olivine. Figure 8 shows molar An (An = atomic Ca/(Ca + Na + K) x 100) of plagioclase. Figure 9 shows the molar Mg# of clinopyroxene.

Orthopyroxene

The molar Mg# compositions of orthopyroxene are shown in Fig. 5. The Pseudoreef Unit pyroxenite contains the most magnesian orthopyroxene primocrysts and the largest range in Mg# (79 to 85). Orthopyroxene shows a similar chemical variation in the normal pyroxenites and pegmatoids of the Merensky Unit (Mg# 79 to 82). There are some differences between the normal pyroxenites and the pegmatoids with the latter having an average orthopyroxene Mg# of 80–82 whereas the normal pyroxenites have a lower average orthopyroxene Mg# of 79 (with the exception of sample 3–9 which has an average orthopyroxene Mg# of 81). The UG-2 Unit and Bastard Unit pyroxenites show strong similarity with Mg# of orthopyroxene ranging between 80 and 81. Euhedral orthopyroxene primocrysts in the FW3 norite to the Merensky Unit have an average Mg# of 82. Anhedral orthopyroxene oikocrysts present in the Mid2-3 anorthosites have average Mg# compositions of 72 to 74.

Olivine

The molar Fo compositions of olivine are shown in Fig. 5. Olivine shows limited variation in Fo composition vertically and laterally, as well as from the core to rims of individual grains. Olivine in the UG-2 Unit pyroxenite has an average composition of Fo_{78-79}. Olivine in the Pseudoreef Unit pegmatoidal pyroxenites has an average composition of Fo_{80-81}. Olivine in the FW5-6 anorthosites to the Merensky Unit has an average composition of Fo_{81}. Olivine in

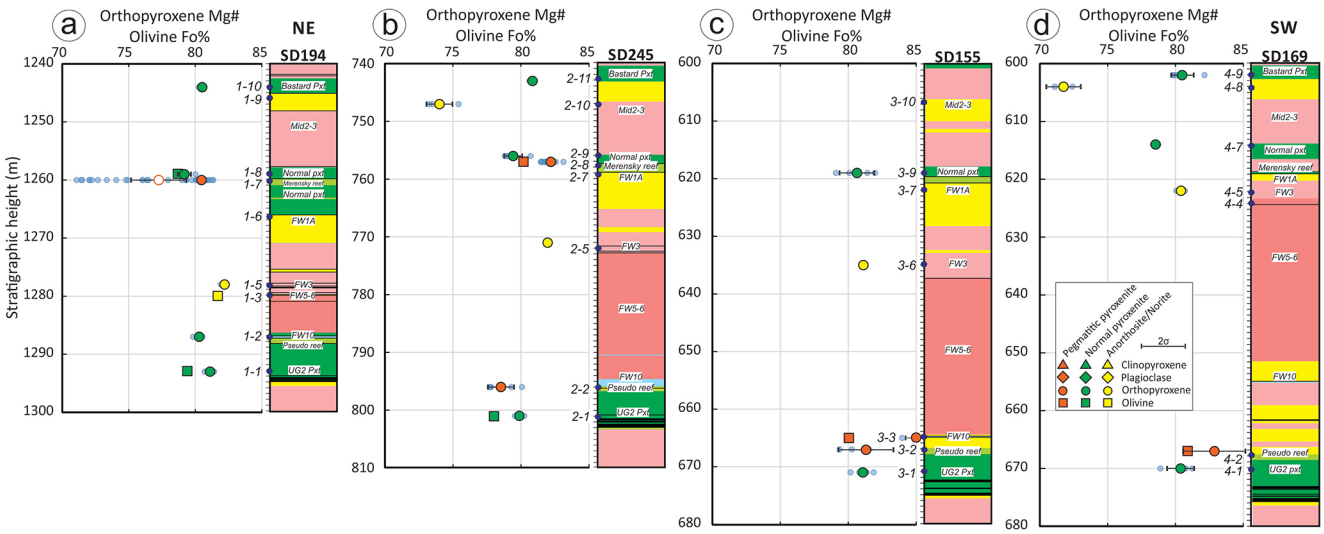

Fig. 5 Fo of olivine and molar Mg# of orthopyroxene as a function of stratigraphic height in the four drillcores at Styldrift Mine (Impala Bafokeng). (**a**) SD194; (**b**) SD245; (**c**) SD155; (**d**) SD169. Average values are emphasised in the legend, and all values are shown as blue circles

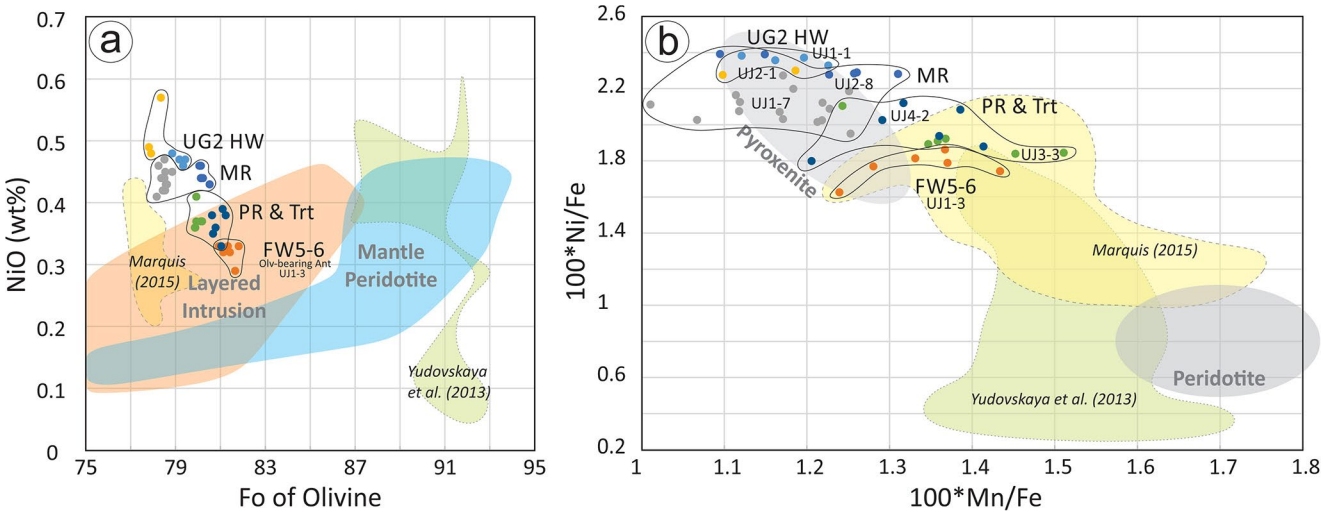

Fig. 6 Olivine compositions for the Styldrift Mine (Impala Bafokeng) samples are shown in comparison to other published olivine data for the Bushveld Complex. (**a**) NiO (wt %) vs. Fo (**b**) 100 x Mn/Fe vs. 100 x Ni/Fe plot. Areas of olivine compositions from peridotite and pyroxenite mantle sources are from Sobolev et al. (2007)

the Merensky Unit pegmatoidal pyroxenites has an average composition of Fo_{78-80} (Fig. 5a-b). There is no significant variation in CaO or MnO (wt%). Olivine is highly enriched in NiO (wt%) compared to olivine in the Platreef (Fig. 6a) and falls in the range of pyroxenite mantle rocks (Fig. 6b). There is minor variation in the NiO content of olivine in different layers (Fig. 6a). Olivine in the Pseudoreef Unit pyroxenite generally has lower NiO contents (for the same Fo) compared to the UG-2 and Merensky Unit pyroxenites. Figure 7 shows the compositional variation of an amoeboid olivine inclusion (Fo_{78-79}) in an orthopyroxene megacryst.

Plagioclase

The molar An composition of plagioclase is shown in Fig. 8. Interstitial plagioclase in the normal coarse-grained pyroxenites shows large variation in molar An composition, especially in the pegmatoidal pyroxenites (Fig. 8). Interstitial plagioclase in the Pseudoreef and UG-2 pyroxenite shows molar An compositions ranging between 44 and 71. The Pseudoreef samples generally show more limited variation in An contents as compared to the Merensky samples. Interstitial plagioclase in the Merensky pegmatoids shows similar variations in molar An content (69 to 77) as the overlying normal Merensky pyroxenites (66 to 76). Interstitial plagioclase in the Bastard Reef pyroxenite has similar molar An compositions to the Merensky normal pyroxenites ranging between 69 and 74. Cumulus plagioclase laths in the FW5-6, FW3, FW1A and Mid2-3 anorthosite and norite show a markedly narrower range in molar An compositions between 75 and 77 and show no up-section differentiation (Fig. 8).

Clinopyroxene

The molar Mg# compositions of clinopyroxene are shown in Fig. 9. Interstitial clinopyroxene in the UG-2 pyroxenite has molar Mg# compositions ranging between 79 and 84. Interstitial clinopyroxene in the pegmatoids in the Pseudoreef has an average molar Mg# composition of 76. Interstitial clinopyroxene in the Merensky normal pyroxenite has molar Mg# compositions ranging between 85 and 87. Interstitial clinopyroxene in the Merensky pegmatoid shows a similar range in molar Mg# composition (78 to 86), albeit with fewer analyses. Interstitial clinopyroxene in the Bastard pyroxenite has molar Mg# compositions ranging between 77 and 86. Interstitial clinopyroxene in FW3 and FW5-6 anorthosite has a very limited range in Mg# composition (average Mg# of 85). Interstitial clinopyroxene in FW1A anorthosite has molar Mg# compositions between 71 and 75. Interstitial clinopyroxene in the Mid3 norite has molar Mg# compositions between 78 and 82.

Strontium isotopes in plagioclase

The strontium isotope data are shown in Fig. 10. There are lateral variations in the initial (at 2.06 Ga) $^{87}Sr/^{86}Sr$ composition of plagioclase in the normal pyroxenites and pegmatoidal pyroxenites with the average initial $^{87}Sr/^{86}Sr$ composition of plagioclase decreasing from ~0.7072 to ~0.7066 from northeast to southwest. The pegmatoidal pyroxenites show a similar trend, at least between drillcores SD194 and SD-245. The initial $^{87}Sr/^{86}Sr$ compositions of plagioclase in the normal pyroxenites are similar to the initial $^{87}Sr/^{86}Sr$ compositions of plagioclase in the pegmatoidal pyroxenites in drillcore SD-194. However, there are slight

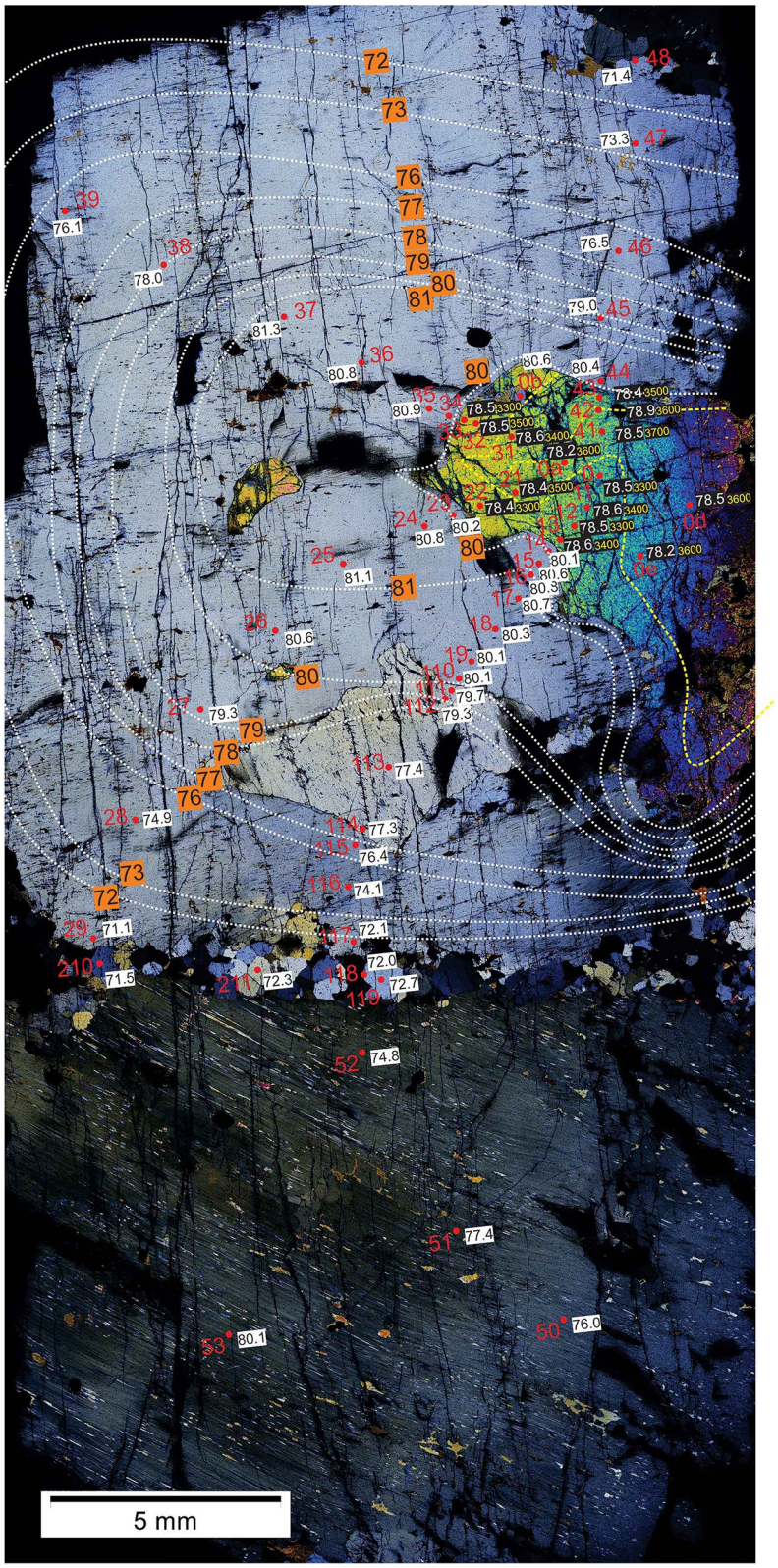

Fig. 7 A full thin section scan of two orthopyroxene megacrysts separated by a thin (~1 mm) chain of fine-grained orthopyroxene grains. The upper orthopyroxene megacryst contains an amoeboid olivine inclusion. The Fo and Mg# compositions are plotted (the points in red text correspond to the spot number). Note the fine grains of orthopyroxene are in compositional equilibrium with the rim of the adjacent megacryst. Mg# contours (dashed white lines) are shown with Mg# bins (the values in orange boxes) indicating an increasing Mg# of orthopyroxene towards the olivine inclusion

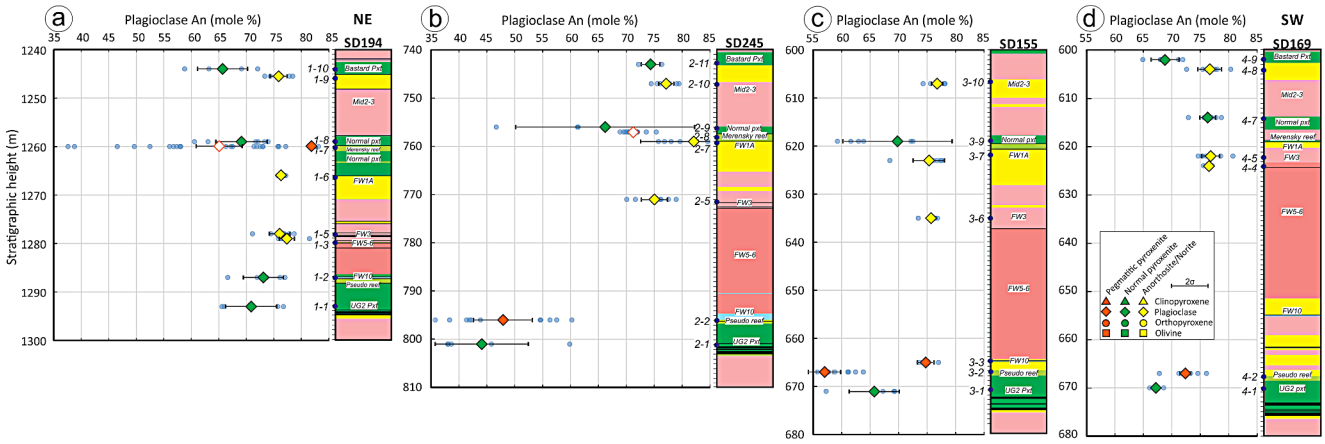

Fig. 8 Molar An composition of plagioclase as a function of stratigraphic height in the drillcores at Styldrift Mine (Impala Bafokeng). (**a**) SD194; (**b**) SD245; (**c**) SD155; (**d**) SD169. Average values are emphasised in the legend, and all values are shown as blue circles

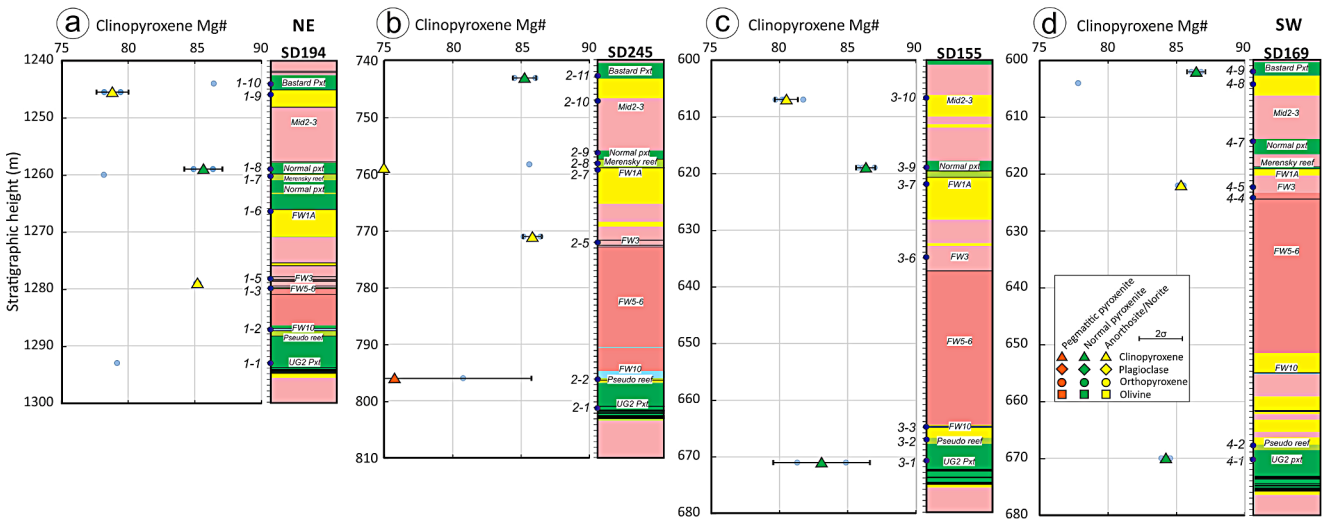

Fig. 9 Molar Mg# of clinopyroxene as a function of stratigraphic height in the drillcores at Styldrift Mine (Impala Bafokeng). (**a**) SD194; (**b**) SD245; (**c**) SD155; (**d**) SD169. Average values are emphasised in the legend, and all values are shown as blue circles

differences in drillcore SD-245. There is large inter- and intra-grain variation in the initial $^{87}Sr/^{86}Sr$ of plagioclase in most of the samples. For example, the Merensky pegmatoid contains highly irregularly zoned interstitial plagioclase oikocrysts with initial $^{87}Sr/^{86}Sr$ ranging between 0.707 and 0.708 (e.g., Fig. 11). Very similar inter and intra-grain variation in the initial $^{87}Sr/^{86}Sr$ of plagioclase is observed in the normal pyroxenites. Cumulus plagioclase laths in the footwall anorthosite to the Merensky Reef in SD-194 show similar initial $^{87}Sr/^{86}Sr$ of plagioclase compositions to the Merensky pyroxenites. The outlier is the hangingwall anorthosite to the Bastard Unit with the least radiogenic cumulus plagioclase compositions (~0.706).

Discussion

The petrogenesis of pegmatoids in the Merensky Reef is still not fully understood. Some researchers have suggested a close relationship between the spatial distribution of the PGE mineralisation and the pegmatoidal textures in the Merensky Reef (Viljoen 1999; Campbell et al. 1983; Prevec 2018). This suggests that understanding the petrogenesis of the pegmatoids is crucial towards understanding the origin of the PGE metallogenesis. This is further emphasised by the lack of pegmatoidal textures in the subeconomic Bastard Reef (Lee and Butcher 1990). In this section, we provide a summary of the previous models for the formation of the Merensky pegmatoids before we use our data to provide a new model. We then elaborate on the important implications for the morphology of the chamber and the metallogenetic processes.

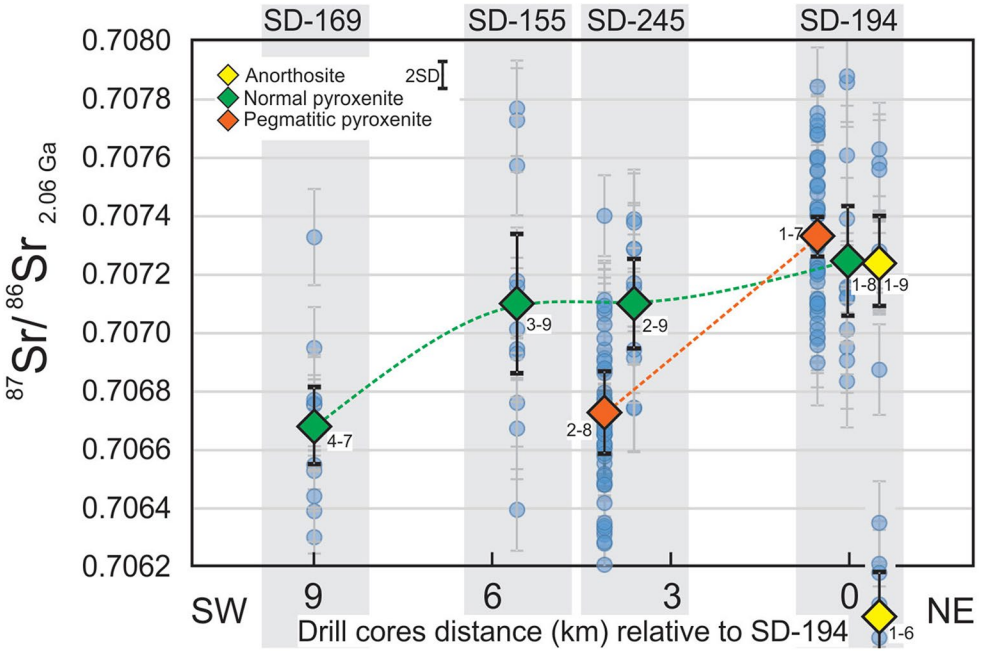

Fig. 10 Variations in the initial (at 2.06 Ga) $^{87}Sr/^{86}Sr$ composition of plagioclase in the drillcores at Styldrift Mine (Impala Bafokeng)

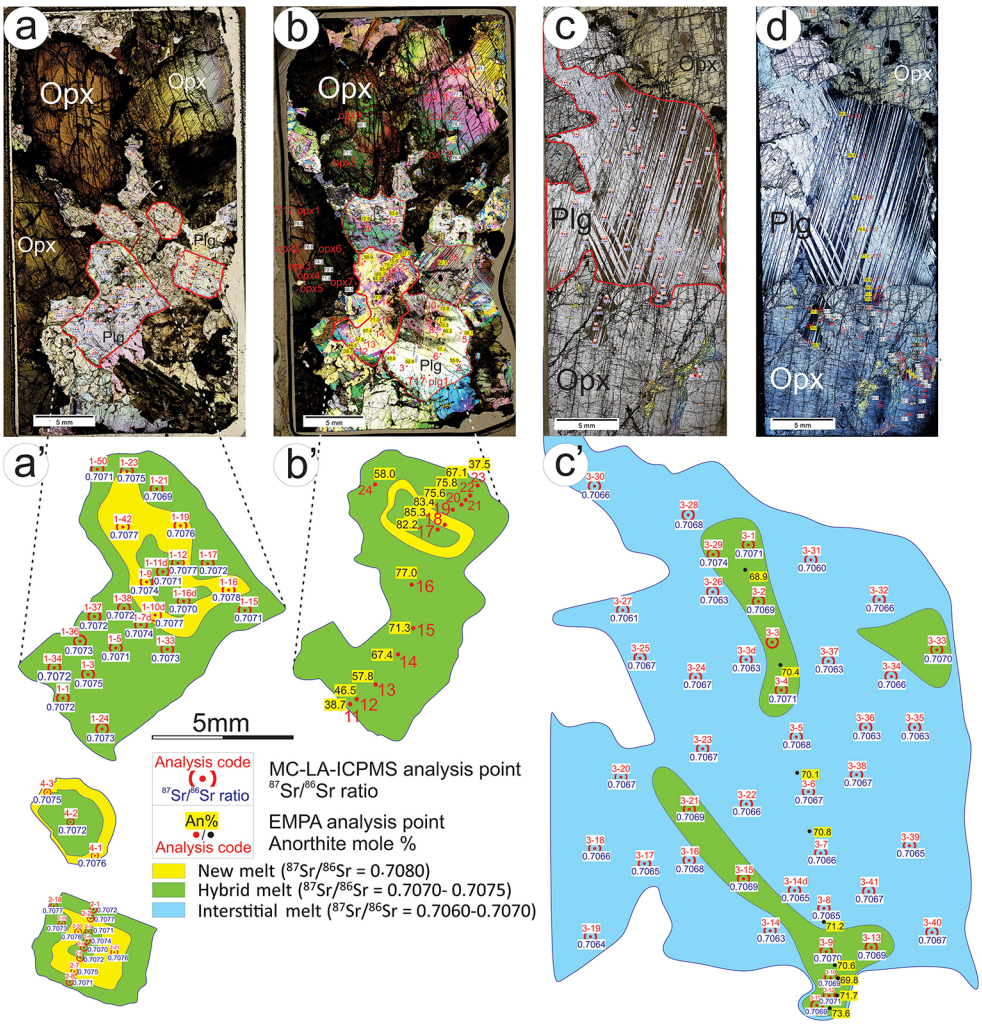

Fig. 11 Four full thin-section scans are shown for Merensky pegmatoids. **(a)** sample 1-7tk from SD194; **(b)** sample 1-7tn from SD194; **(c, d)** sample 2-8 from SD245. The interstitial plagioclase oikocrysts were analysed in detail with molar An and initial $^{87}Sr/^{86}Sr$ compositions shown in a', b', and c'

Previous hypotheses for the origin of the Merensky Reef pegmatoids

Various models have been proposed for the origin of the Merensky pegmatoids. Some have suggested that volatiles were important in developing the pegmatoidal textures (e.g., Lauder 1970; Vermaak 1976; Irvine et al. 1983; Nicholson and Mathez 1991; Mathez et al. 1997; Boudreau 1999; Wilson et al. 1999; Mathez and Kinzler 2017; Maier et al. 2021). Vermaak (1976) proposed there were floating mats of plagioclase in the chamber that trapped successive magmas (and volatiles) beneath them. The volatiles fostered the rapid growth of ferromagnesian minerals that aggregated into boulder-like masses that settled to the chamber floor to produce the pegmatoidal facies.

Nicholson and Mathez (1991) and Maier et al. (2021) suggested that the Merensky Reef was initially a melt-rich proto-reef (i.e., orthocumulate) between the hangingwall pyroxenite and underlying norite. They suggested that the annealing process only began when volatiles were introduced to a high porosity orthocumulate horizon. Campbell et al. (1983) suggested that the pegmatoids had a lower solidus temperature because of their greater porosity, so they acted as a trap for volatiles and incompatible elements facilitating crystal growth compared with the surrounding normal pyroxenite. In all these models, it is implied that volatile introduction into the proto-melt-rich reef resulted in orthopyroxene-plagioclase melting (by the expansion of the olivine field). However, the problem with these models is that there is no intrinsic reason why the orthopyroxene-rich orthocumulate layer (i.e., the proto-reef) should be more porous, and hence melt-rich, in the first place (Arndt et al. 2005). Volatiles may have played a possible role in the concentration and deportment of PGEs in the Merensky Reef (Prevec et al. 2021), although, this process needs to be accompanied by a driving force such as a flowing silicate melt (e.g., a hydrous melt) for unlocking and fluidising the crystal mush and to produce an orthocumulate layer and trap volatiles (e.g., Campbell et al. 1983). Volatiles alone cannot be expected to generate uniform PGE mineralisation across a massive intrusion like the RLS.

Viljoen (1999) proposed that the pegmatoids formed by the "reconstitution" of the normal pyroxenites. Slow cooling and textural annealing were proposed by Cawthorn and Boerst (2006). In their model, the pegmatoids represent a prolonged period of crystal growth before the deposition of the normal pyroxenites above. Wilson and Chunnett (2006) seemed to argue for a quenching model when two magmas mixed, similar to that of Ballhaus and Ryan (1995), but they explicitly link this to the harrisitic olivine and fine-grained layers of pyroxenite. A combined slow-cooling and volatile model was suggested by Latypov et al. (2015). They argued the Merensky pegmatoids formed by the melting and dissolution of earlier formed cumulates because of successive pulses of superheated magma, which is similar to the model proposed by Viljoen (1999).

We discard the notion of a slow-cooling cumulate hypothesis, as described above, as there is no justification for the presence of a substantial overlying melt-body, as is elaborated upon in the next section. We also rule out the porosity hypothesis of Campbell et al. (1983) using the same reasoning that Arndt (2005) used, that is, there is no intrinsic reason why the pegmatoids had a higher initial porosity. While volatiles in the magma may have exerted a minor influence on crystal growth, as shown by the relatively greater abundance of hydrous minerals in the Reef, it is crucial to note that according to Prevec et al. (2021), volatiles alone are insufficient to produce the required PGE grades, and there is little evidence of fluids redistributing PGE due to a lack of correlation between mobile elements (e.g., K-Rb) and PGE (Wilson and Chunnett 2006). Also, the PGE grades demand an orthomagmatic driving force such as a flowing silicate melt (e.g., a hydrous melt) to unlock and fluidise the mush (e.g., Bergantz et al. 2015) and hence expose sulfide melts to high volumes of silicate melt for metal tenor upgrading. Therefore, we preclude any kind of volatile-driven model for the origin of the PGE mineralisation which leads us to favour an orthomagmatic model. The correlation of greater PGE grades and greater thicknesses of the Reef indicate the mineralisation process and rock-forming process are inextricably linked. Furthermore, the PGE metal tenors are greater in the northeast and decrease towards the southwest (unpublished data). The lateral variations in the composition of the orthopyroxene megacrysts and the strong chemical (An-$^{87}Sr/^{86}Sr$) zonation of interstitial plagioclase strongly indicate to us that lateral melt flow and mixing played a pivotal role in the development of the pegmatoids in the Merensky Reef.

Some authors have stated that the pegmatoid-forming process is closely linked to the mineralisation process (e.g., Viljoen 1999; Prevec et al. 2021), however, the link between how the pegmatoids formed and the origin of the PGE mineralisation is unclear in many of the pegmatoid-forming models presented in the literature. In the volatile-based models, it has been argued that the sulfur and PGE were carried in hydrothermal fluids – so the agent causing crystal growth may have simultaneously deposited PGE-enriched sulfide. In the orthomagmatic models for the formation of the pegmatoids, one can attribute the formation of PGE-enriched sulfide to magma mixing, high-R-factors and the settling of the sulfide with the major silicate minerals. The rate at which the pegmatoid cooled would merely lead to the coarsening of the primocrystic framework and not affect the interstitial sulfide material. The reality is that a combination

of magmatic and hydrothermal processes were involved in the petrogenesis of the Merensky Reef (e.g., Smith et al. 2021). In the next section, we use our textural and mineral compositional constraints to provide a new hypothesis for the origin of the Merensky pegmatoids.

The origin of the Merensky Reef pegmatoids by melt infiltration in a crystal mush

Textural constraints

The pyroxenites of the Merensky Reef, as well as the Pseudoreef and Bastard Unit, are dominantly poikilitic in texture (Fig. 4). The pegmatoidal facies are also poikilitic with inclusions of olivine, plagioclase, and chromite common in the orthopyroxene megacrysts. Chromite inclusions are also common in interstitial plagioclase in both the normal pyroxenites and the pegmatoids. The Merensky Reef is relatively rich in accessory phases such as phlogopite, K-feldspar, quartz, apatite, and zircon. The combination of the poikilitic textures, and the presence of low-temperature mineral species, imply a complex petrogenetic evolution for the Merensky Reef.

The presence of amoeboid olivine inclusions (e.g., Fig. 4h') in the orthopyroxene megacrysts provides insights into the earliest crystallisation dynamics of the Merensky Reef. Plagioclase inclusions have straight-grain boundaries with the amoeboid olivine grains (e.g., Fig. 4i') that suggests there was a cotectic relationship between these two phases before the crystallisation of orthopyroxene. The molar Mg# composition of the surrounding orthopyroxene grain increases towards the amoeboid olivine inclusions (Fig. 7). We interpret this as the product of a peritectic reaction caused by the olivine primocryst reacting with a relatively silica-rich melt (as documented in the MG-1 chromitites by Kaufmann et al. 2018). The olivine primocryst was resorbed and orthopyroxene grew from the melt to envelop the amoeboid olivine. The enveloping orthopyroxene shielded the relict olivine from the melt, terminating and preserving the peritectic reaction. This peritectic transformation included the solid-state diffusion of Mg cations from the relict olivine to the adjacent orthopyroxene, giving the neighbouring orthopyroxene its lower Fe/Mg and producing the observed chemical profile in Fig. 7 (Zellmer et al. 2016).

The orthopyroxene megacrysts in the pegmatoids are commonly surrounded by thin chains of fine-grained orthopyroxene (e.g., Fig. 7). The finer-grained orthopyroxene has molar Mg# compositions in equilibrium with the rims of the adjacent orthopyroxene megacrysts. Individual crystals of the fine-grained orthopyroxene may also show very subtle reverse zoning (e.g., points #118 and 119 have molar Mg# compositions of 72.7% and 72%, respectively: see Fig. 7). We interpret these fine-grained orthopyroxene crystals to have formed by dissolution-reprecipitation (pressure solution) in the presence of a silicate melt (Holness et al. 2017).

In summary, the textural evidence implies that there was dynamic recrystallisation in the presence of silicate melt during the solidification of the Merensky pegmatoids.

Mineral compositional constraints

Orthopyroxene primocrysts in the normal pyroxenites show constant molar Mg# compositions laterally over a 10 km distance at Styldrift Mine (Fig. 12a). Conversely, the orthopyroxene megacrysts in the pegmatoids appear to show increasing molar Mg# compositions from the northeast to the southwest (Fig. 12b). This may also be the case for the molar Fo compositions olivine inclusions in the pegmatoids although there may be too few analyses to make this interpretation (Fig. 5a). It is also noted that the molar Mg# compositions of orthopyroxene are very similar between the UG-2, Merensky and Bastard pyroxenites (Fig. 5). We do not consider the lateral molar Mg# (and Fo) compositional trends to be strictly the products of the "trapped liquid shift effect" (Cawthorn 2015) as there is a poor correlation between the modal abundance of orthopyroxene and Mg#. Also, the Pseudoreef samples (#2–2, 3 – 2, and 4 – 2) contain the highest proportions of interstitial plagioclase (i.e., trapped melt) and they contain orthopyroxene grains with higher Mg# compositions compared to more orthopyroxene-rich samples. These relations suggest to us that the orthopyroxene and olivine compositions, certainly their cores, are primary magmatic signatures.

Interstitial plagioclase oikocrysts in the pyroxenites were formed by the crystallisation of pore melt and will therefore record any evidence of melt-crystal reactions after the accumulation of the framework of orthopyroxene primocrysts. The plagioclase oikocrysts are strongly zoned in molar An composition (An_{37-85}) and initial $^{87}Sr/^{86}Sr$ (0.706 to 0.708). This is apparent in individual samples. The plagioclase oikocrysts become more calcic up-dip in the pegmatoids over a distance of 10 km from the northeast to the southwest (Fig. 12c-d). This is particularly evident in the Pseudoreef, where the molar An composition of plagioclase increases by more than 20 mol% An units from the northeast to the southwest (Fig. 12d). Interstitial plagioclase in the normal pyroxenites shows relatively constant molar An compositions laterally, although they may increase by ~5 mol% An units from the northeast to the southwest in the Merensky pyroxenite (Fig. 12c). The plagioclase oikocrysts show a decrease in their initial $^{87}Sr/^{86}Sr$ composition from the northeast to the southwest in both the normal pyroxenites and the pegmatoids (Fig. 10).

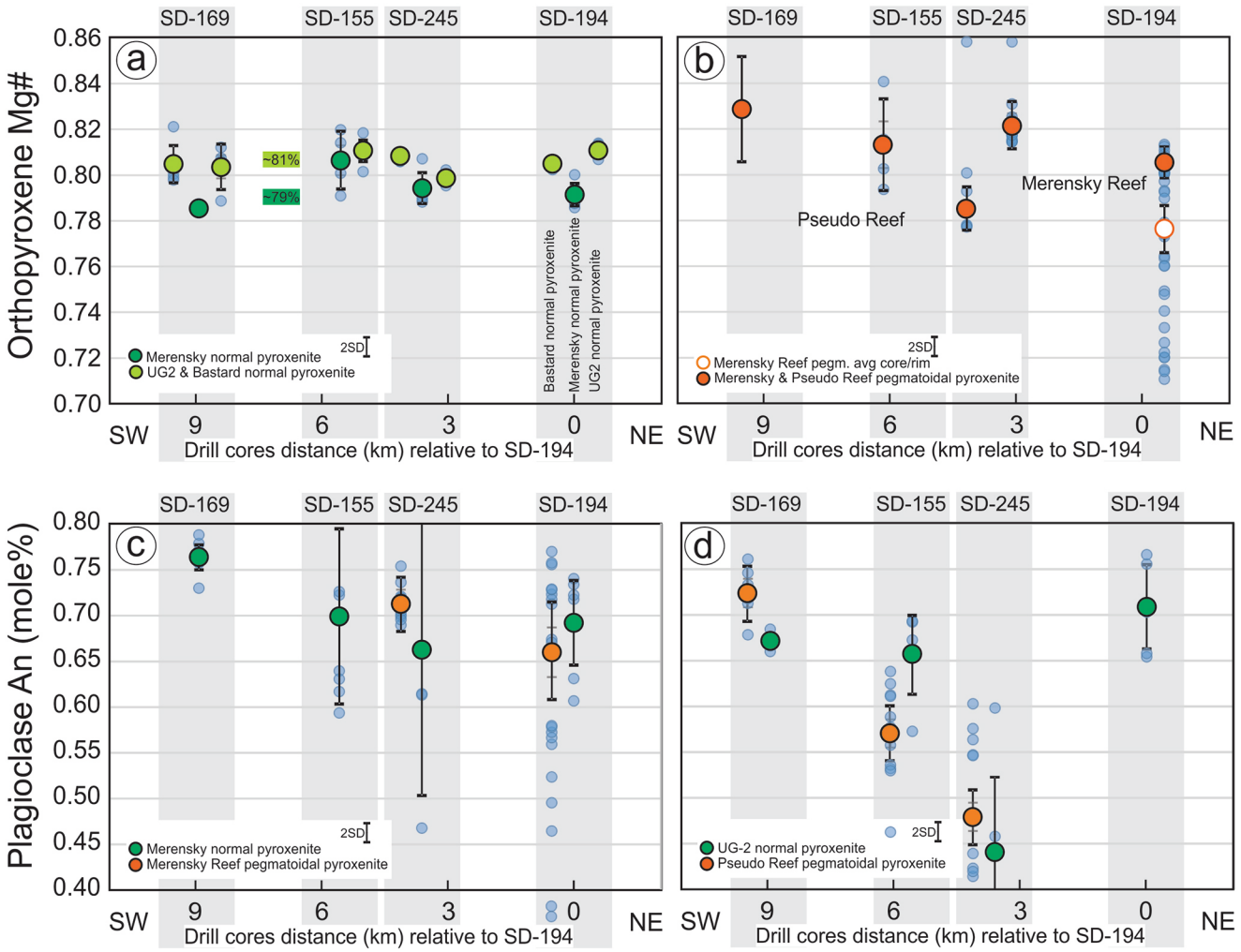

Fig. 12 A summary plot of the along dip (northeast to southwest) variations in the molar Mg# of orthopyroxene (**a**, **b**) and molar An of plagioclase (**c**, **d**) in the four drillcores at Styldrift Mine (Impala Bafokeng)

Individual plagioclase oikocrysts display complex zonation in strontium isotopic composition. Such strong isotopic disequilibrium can be expected considering the bulk rock variations in Sr-Nd isotopes (e.g., Kruger 2005; Sharpe 1985; Lee and Butcher 1990; Maier et al. 2000), mineral-scale variations in Sr-Nd isotopes (e.g., Prevec et al. 2005; Seabrook et al. 2005; Chutas et al. 2012), and localised trace element disequilibrium (e.g., Wilson and Chunnett 2006) in the Merensky Reef. Complex Sr-isotope zoning is apparent in the plagioclase oikocrysts from the Merensky pegmatoids as shown in Fig. 11. The plagioclase oikocrysts from the northeastern pegmatoids show radiogenic domains (initial $^{87}Sr/^{86}Sr$ = 0.708) surrounded by less radiogenic domains (initial $^{87}Sr/^{86}Sr$ = 0.707 to 0.705: Fig. 11a'). The more radiogenic plagioclase domains are also characterised by high molar An compositions (e.g., An_{82-85}: Fig. 11b') at least in the Merensky Reef. The plagioclase oikocrysts from the southwestern pegmatoids show relatively fewer radiogenic domains (initial $^{87}Sr/^{86}Sr$ = 0.707 to 0.705) surrounded by relatively more radiogenic domains (initial $^{87}Sr/^{86}Sr$ = 0.707 to 0.706) with no apparent variation in molar An compositions (Fig. 11c'). The extreme range of molar An compositions of plagioclase oikocrysts, along with their complex zoning in $^{87}Sr/^{86}Sr$, in the pegmatoids, suggests they had a more prolonged cooling history relative to the normal pyroxenites. We suggest this is because the pegmatoidal zones were facilitating for longer the percolation of isotopically distinct melts and allowing for the final trapped melt to fractionate to greater Na/Ca compositions giving rise to more sodic plagioclase compositions.

A new hypothesis for the origin of the Merensky Reef pegmatoids

The regional (km-scale) mineral-scale variations in major element and isotopic compositions at Impala Bafokeng

are indicative of lateral melt infiltration in a crystal mush in which compositionally diverse melts reacted with earlier-formed crystals. We suggest that the pegmatoids were formed in response to this process. We favour such a hypothesis largely because of the challenges involved in explaining the lateral variability in mineral composition by either the mechanical accumulation or in situ nucleation of crystals on a chamber floor. It is also difficult to explain these features by the injection of a basal flow of melt along the chamber floor (e.g., Naldrett et al. 2009) because the resultant melt composition would rapidly homogenize and give rise to compositionally homogeneous cumulates along the chamber floor. The olivine-orthopyroxene reaction textures, fine-grained orthopyroxene chains, and the complex Sr isotopic zonation in the plagioclase oikocrysts would also not develop in such a scenario. Instead, we explain the development of the lateral textural and mineral compositional variations as a response to melt infiltration in a crystal mush. The ambient mushy environment into which the melt infiltrated would have been relatively hot (i.e., supra-solidus), so it would not have quenched/chilled upon emplacement. As for the driving force, and why melt infiltrated at this particular horizon, we can only speculate that this was driven by the buoyancy of the magma and the presence of a rheological weakness at time level of the chamber (i.e., melt-bearing crystal mush). The detail of our model is shown schematically in Fig. 13.

The presence of amoeboid olivine inclusions in textural equilibrium with plagioclase shows the initial presence of a troctolitic crystal mush at the level of the Merensky Reef as has been suggested by others (e.g., Boudreau 1999; McDonald et al. 2005; Yudovskaya et al. 2013; Maier et al. 2021). The troctolitic crystal mush may have been the early solid products of the injection of a magnesian basalt into a resident feldspathic cumulate pile (e.g., Mungall et al. 2016; Mitchell et al. 2019; Mansur and Barnes, 2020; Maghdour-Mashhour and Hayes 2021). The lower chromitite stringer was also formed around this time either by the mixing of the incoming magnesian basalt with the resident feldspar-saturated pore melt in the crystal mush (e.g., Irvine, 1977) or by the viscous segregation of chromite from the mush (assuming chromite was a phenocryst in the injected melt) (e.g., Marsh et al. 2013). Both processes are depicted in Fig. 13a because the lower chromitite stringer appears to contain coarse-grained and fine-grained chromite. The fine-grained chromite may be products of pore-scale melt mixing and the coarse-grained chromites may be the result of viscous segregation.

The troctolitic crystal mush was then replenished by channelised flow of a relatively silica-rich and hydrous melt which was probably “B2”, a mixture of komatiite, continental crust, and a plagioclase-rich residuum (Barnes et al. 2010). Wilson and Chunnett (2006) noted from their extensive trace element dataset for the Merensky Reef that these cumulates are the products of hybridised magmas (i.e., mixtures of B1 and B2 melt). The new melt infiltrated the crystal mush, dissolving the olivine primocrysts and precipitating the orthopyroxene megacrysts. The infiltrating melt was more evolved (lower Ca/Na) and more radiogenic in terms of its strontium isotopic composition compared to the pore melts in the resident crystal mush. The infiltrating melt must have therefore had a distinct crustal contamination history compared with the pore melts in the mush. The lateral variation in the mineral compositions of the pegmatoids and their host “normal” pyroxenites are largely decoupled in that orthopyroxene (molar Mg#) and olivine (Fo) compositions increase in the pegmatoids laterally away from the feeder whereas they remain largely constant in the “normal” pyroxenites. This demonstrates that the pegmatoids have a distinctive magmatic history compared to the host “normal” pyroxenites. We suggest that the lateral increases in molar Mg# of orthopyroxene and Fo of olivine reflect the residency time of the percolating melt in the mush. This residency time was greater towards the northeast as it is closer to the inferred magma feeder where it was hotter. Therefore, the crystal mush closer to the feeder experienced a more prolonged timescale of melt-crystal interaction allowing for an increase in Fe/Mg in orthopyroxene megacrysts nearer the feeder. This is shown by the more extreme molar An zoning of plagioclase oikocrysts in the northeastern pegmatoids that reflect deeper fractionation and melt evolution.

Melt infiltration switched from a more channelised style to a more porous style presumably because of the loss of heat and kinetic energy further away from the feeder. A more crystal-rich mush distal to the feeder would have forced melt infiltration to be more porous flow in style. This can also explain the better preservation of the resident pore melt compositions in this region. Interstitial plagioclase oikocrysts in the normal pyroxenites are also characterised by extreme zoning in initial $^{87}Sr/^{86}Sr$ compositions similar to that observed in the pegmatoids. This may have been caused by the percolation of melt into the overlying hangingwall pyroxenite mush, during melt infiltration as has been shown during the accretion of the MG3F anorthosite layer at the LCZ-UCZ boundary (Maghdour-Mashhour et al. 2021). Melt replenishment into the Merensky crystal mush also speaks to the presence of relatively evolved accessory minerals, especially zircon. The Merensky Reef contains relatively abundant zircon, as does its counterparts in the Northern Limb (i.e., Platreef-Flatreef), which are probably correlative based on their similar lithology (e.g., Barnes and Maier, 2002; Yudovskaya et al. 2017; Grobler et al. 2019). The protracted crystallisation timescales recorded in zircon grains from the Merensky Reef, and for the rest of the Upper

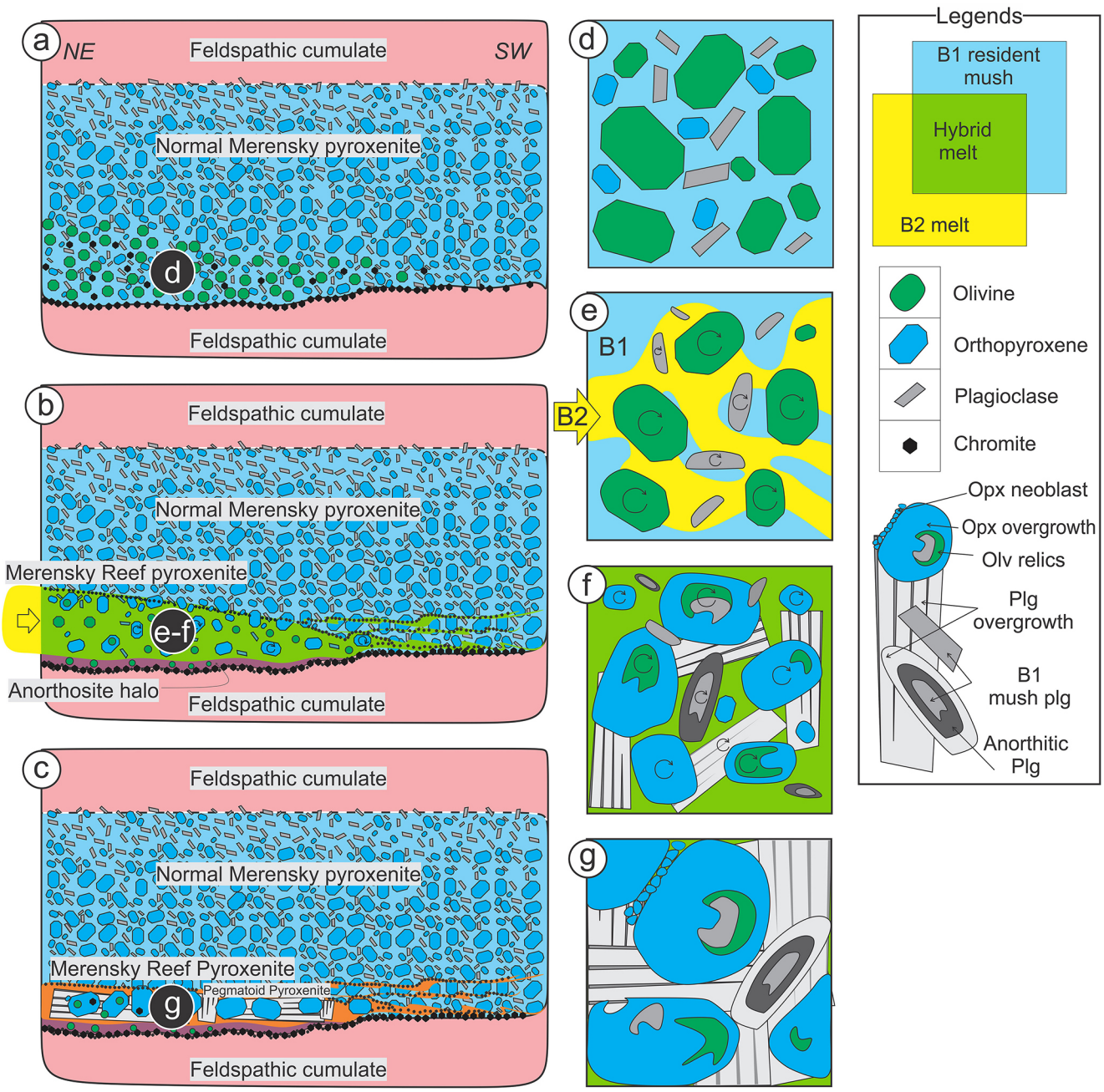

Fig. 13 A cartoon illustrating our melt infiltration model for the petrogenesis of the Merensky Reef pegmatoids. (**a**) There was an initial pyroxenitic mush, which was olivine and chromite bearing at its base, that eventually goes on to form the "normal" Merensky pyroxenite. This may have been formed as an intrusion into a resident feldspathic cumulate (as suggested by Mungall et al. 2016 and others). The lower chromitite stringer was formed at this point by mixing between pore melts derived from the pyroxenite and the resident feldspathic cumulates as well as by the viscous segregation of chromite grains in the mush. (**b**) The pyroxenitic/troctolitic crystal mush was invaded by an infiltrating Si-rich melt (i.e., B2 melt after Barnes et al. 2010). Melt infiltration was channelised near the magma feeder and porous distally to the feeder. It is this melt infiltration process that leads to the dissolution-reprecipitation processes in the resident crystal mush and the development of the coarse-grained to pegmatitic textures. (**c**) The fully solidified Merensky Unit showing well developed pegmatoid layers near the feeder and patchy pegmatoid further away from the feeder. Parts (**a**), (**b**), and (**c**) are annotated with parts (**d**), (**e**), (**f**) and (**g**) that show the granular-scale details of the melt infiltration and dissolution-reprecipitation processes

Critical Zone (Mungall et al. 2016; Scoates et al. 2022), can be interpreted to reflect the prolonged presence of a melt component or as the result of influxes of replenishing melt that buffered or raised the temperature of the melt above the zircon closure temperature in the Merensky crystal mush. This is consistent with our model for melt infiltration during the solidification of the Merensky Reef.

Our hypothesis for the origin of the pegmatoidal textures, and the lateral variations in mineral composition, is similar to the "cumulate reconstitution" processes suggested by previous researchers (e.g., Viljoen 1999; Cawthorn and Boerst 2006; Latypov et al. 2015). However, a corollary of the cumulate reconstitution hypothesis, and the other models discussed above, is that the Merensky Reef formed at the base of a melt-filled magma chamber. We propose that this cumulate reconstitution and pegmatoid formation was driven by melt infiltration in a crystal mush. This has important implications for the morphology of the RLS during the solidification of the Merensky Reef, which we discuss next.

The morphology of the 'chamber' during the petrogenesis of the Merensky Reef

There has been a paradigm shift in our understanding of the accretion mechanisms of igneous layering in the RLS. The traditional view is that the igneous layering (and the stratiform ore deposits) in the RLS were the products of the sequential cooling and crystallisation of a large, periodically replenished melt-rich chamber with either the mechanical segregation of crystals or their heterogenous nucleation (e.g., Cawthorn 2015) and this view has been championed by Latypov et al. (2022). Detailed geochemical, geochronological, and field-based studies instead show that igneous layering in the RLS may be the product of the non-sequential emplacement of magmas in a mushy or cumulate pile resident in the chamber (e.g., Mungall et al. 2016; Hayes et al. 2018; Mitchell et al. 2019; Maghdour-Mashhour et al. 2021; Scoates et al. 2021). It is implied from this interpretation that the layered sequence is not necessarily constructed of younger layers on top of older layers. This raises significant questions about the traditional view of the existence of a large molten chamber during the solidification of the RLS.

The lateral variations in the major element and Sr-isotope composition of minerals from pyroxenites in the Upper Critical Zone at Styldrift Mine imply that the igneous layering (and the Merensky Reef) did not form by sequential crystallisation at the base of a melt-filled magma chamber. Instead, lateral magma replenishment into a crystal mush followed by magma mixing and crystal-melt reactions were important and are supported by the lateral mineral compositional and isotopic variations. Furthermore, there is a remarkable similarity in the molar Mg# compositions of orthopyroxene primocrysts in each of the major pyroxenite layers in the Upper Critical Zone at Styldrift Mine (Fig. 5). This suggests to us that the magma forming each of these pyroxenite layers was very similar in its composition and, therefore, the Upper Critical Zone does not record a sequentially fractionated sequence of cumulate rocks. Instead, there was periodic replenishment of the chamber by new batches of magnesian magma, some of which triggered sulfur saturation and the formation of stratiform PGE deposits.

The previous models for pegmatoid formation, as summarised in the section above, are dependent on the formation of the Merensky Reef at the base of a large melt-filled chamber. The presence of a large melt-filled chamber was deemed necessary to explain the extremely high metal tenors of the sulfides in the Merensky Reef as they would have to equilibrate with large volumes of silicate melt. However, this concept has faced multiple problems such as (i) how the sulfide were able to settle simultaneously across a massive area to produce a single PGE-rich layer, and (ii) the Main Zone (which is presumed to represent the products of the resident melt in the chamber) is not PGE-depleted (e.g., Maier and Barnes 1999), suggesting it was not admixed with the Merensky Reef-forming magmas. Also, in the context of a large melt-rich chamber, which is convecting and continually homogenising in its composition, the Merensky Reef should show limited lateral chemical variability. But this is not the case at Styldrift Mine, where mineral compositional variability is observed along a 10 km interval of the Merensky Reef. On this basis, we argue that our melt infiltration and cumulate reworking model for the origin of the pegmatoids implies that the Merensky Reef formed non-sequentially in a crystal mush. There is evidence that the crystal mush in the Merensky Reef was above its solidus for a relatively prolonged period allowing the pore melt to fractionate to more evolved compositions. Therefore, cumulate material above the Merensky Reef may have been actively crystallising (or was completely solidified) at the time the Merensky Reef was forming. This was proposed by Hayes et al. (2018) who suggested that the Marikana dykes crosscutting the Main Zone represent the expulsion of low-temperature residual melts derived from the Upper Critical Zone.

In summary, there is evidence that the Merensky Reef was not the product of sequential crystallisation in the chamber, and instead may represent a horizon in the chamber that cooled at slower timescales compared to its underlying and overlying cumulates due to its open-system nature with replenishing melts infiltrating this horizon. Such an environment is comparable to conduit-type magmatic systems (e.g., Barnes et al. 2016) and provides new exploration avenues in the search for new types of PGE ore bodies hosted in layered intrusions. Furthermore, pegmatoidal textures are common

throughout the Platreef in the Northern Limb (e.g., Kinnaird 2005; Holwell et al. 2006) and Waterberg PGE deposit in the Far Northern Limb (Kinnaird, 2017 Yudovskaya et al. 2022) suggesting melt infiltration in a crystal mush is a pervasive process across the entire Bushveld Complex. In the final section below, we provide some speculation as to how this process could have influenced sulfide melt formation and metal tenor upgrading.

Some suggestions for understanding the origin of the PGE mineralisation

Two main models are typically proposed to explain the origin of the PGE mineralisation in the Merensky Reef. Perhaps the most widely accepted of these is the orthomagmatic model in which sulfide melt is generated by magma mixing. Magma mixing can induce sulfur saturation and the production of a sulfide melt (e.g., Campbell et al. 1983; Naldrett and von Gruenewaldt, 1989). The other, and perhaps less widely accepted model, considers Cl-rich PGE-bearing hydrothermal fluids produced the mineralisation (e.g., Ballhaus and Stumpfl, 1986; Mathez 1995; Mathez et al. 1997; Nicholson and Mathez 1991; Boudreau 1999; Prevec et al. 2021).

The orthomagmatic model seems reasonable considering the abundant evidence in the literature that the Merensky Reef formed in response to magma replenishment and mixing (see references above), and this is also apparent in the lateral geochemical variations at Impala Bafokeng (this study). However, the orthomagmatic model is premised on the view that there was a large melt-filled chamber at the time the Merensky Reef formed. This is mostly because of the large R-factor required (i.e., the ratio of sulfide melt to silicate melt), so it is assumed that the extremely high PGE metal tenors were generated by the equilibration of the sulfide melt with a thick overlying resident column of silicate melt (e.g., Campbell et al. 1983; Naldrett et al. 1986; Barnes and Campbell 1988; Arndt et al. 2005; Cawthorn and Boerst 2006). However, as explained in the above section, a large melt-filled chamber is not required during Merensky times to explain the origin of its silicates. This is also consistent with the observation that the parent melts to the Main Zone lacked appreciable quantities of PGE (Wilson and Chunnett 2006), so these parent melts could not have upgraded the Merensky sulfides sufficiently to produce the observed metal tenors. Instead, we suggest that sulfide upgrading may have occurred during melt infiltration in a crystal mush. This is supported by a decrease in the Pt metal tenor (in 100% sulfide melt) laterally from the northeast to the southwest at Impala Bafokeng (unpublished data) and is consistent with melt infiltration waning in its efficiency further from the feeder zone.

Perhaps the biggest constraint to sulfide upgrading in a crystal mush is the requirement of a large R-factor to upgrade the PGE metal tenor of the sulfides. The Pt tenor of the Merensky Reef at Impala Bafokeng is up to 450 ppm (unpublished data), so an R-factor of up to 10^5 was required, at least locally. An R-factor of 10^5 implies a volume of silicate melt 1000× greater than the total volume of sulfide melt present in the crystal mush, assuming the interstitial melt in the mush contained ~ 10 vol% sulfide melt prior to melt infiltration. This translates to every 1 mm^3 droplet of sulfide melt equilibrating with 1 cm^3 of silicate melt, and locally up to 1 m^3 of silicate melt, in the case of an R-factors of 10^6 where the metal tenor approaches ~ 1000 ppm (e.g., Mungall et al. 2020). We suggest that such large volumes of silicate melt could have easily infiltrated the crystal mush over a distance of 10,000 m laterally at Impala Bafokeng. Also, the volume of the silicate melt, and hence the R-factor, can be reduced if one considers the possibility that (i) some PGE-rich sulfide was entrained and introduced during melt infiltration (as proposed by Naldrett et al. 2009), and/or (ii) the resident crystal mush was already relatively enriched in PGE, which is possible, considering there are inclusions of platinum-group minerals in the silicates (Ballhaus and Sylvester, 2000). A volume of 10 vol% sulfide melt in the interstitial melt may be too high, especially considering the limit on sulfur solubility in basaltic melt. However, sulfide melt already present in the mush may have been partially dissolved during the upgrade process when exposed to sulfide-undersaturated and PGE-undepleted silicate melts. A two-stage sulfur saturation process is also possible considering the B1 (U-type) melt became sulfur-saturated by crustal contamination of a komatiitic parent melt (Mansur and Barnes, 2020). This B1 liquid would have produced the initial deposition of the troctolitic mush with some sulfide melts. Subsequent pulses of B2 or B3 melts upgraded the sulfide melts in the crystal mush.

The generation of sulfide melt and its upgrading during melt infiltration of a crystal mush is certainly a fruitful avenue of research towards better understanding the origin of PGE-enriched magmatic sulfide deposits. Sulfides in the Merensky Reef tend to be interstitial in texture to the orthopyroxene primocrysts and plagioclase oikocrysts suggesting they were crystallised from the pore melt – and is consistent with our model. These sulfides may have formed and been subsequently upgraded in PGE by equilibration with fresh PGE-undepleted silicate melt percolating through the crystal mush. This possibility is emphasised by the lack of mineable PGE grades in the olivine-rich Pseudoreef.

Conclusion

We present detailed textural and in situ major element and strontium isotope compositions for pyroxenites and their pegmatoids from the Merensky Reef, and wider Upper Critical Zone rocks, from Styldrift Mine (Impala Bafokeng) in the Western Limb of the Bushveld Complex. The presence of amoeboid olivine inclusions in orthopyroxene megacrysts and fine-grained chains of orthopyroxene imply dissolution-precipitation processes during the solidification of the Merensky pegmatoids. The mineral compositional data shows that there is minimal change in the molar Mg# composition of orthopyroxene (and Fo in olivine) along a 10 km interval of cumulates, but that there is extreme variation in the molar An-initial $^{87}Sr/^{86}Sr$ composition of interstitial plagioclase. These findings are consistent with a process of melt infiltration in a crystal mush made up of orthopyroxene (± olivine) primocrysts. Styldrift Mine is in proximity to an inferred magmatic feeder, a structural weakness that was likely exploited by the significantly younger Pilanesberg Complex. We infer that melt replenishment into the resident mush was channelised in proximity to the feeder at the northeastern region and became more porous distal to the inferred feeder. Our findings show that the resident chamber did not need to be a large melt-filled environment during the petrogenesis of the Merensky Reef and suggest to us that the ore-forming processes were heavily influenced by the mixing of melts in a crystal mush. This process had the potential to upgrade the metal tenors of the sulfide and produce the PGE-rich ore deposit. The nature of the petrogenesis of the pegmatoids is therefore crucial towards understanding the metallogenesis of stratiform PGE reefs in large, layered intrusions.

Supplementary Information The online version contains supplementary material available at https://doi.org/10.1007/s00126-024-01278-z.

Acknowledgements We thank Christian Reinke at Spectrau at the University of Johannesburg for his able assistance with the electron microprobe. We also thank Caiphas Majola, Sam Tshabalala and Louis Mudalahothe for technical support at Wits. Constructive and thoughtful reviews of the manuscript by Wolf Maier, Steve Prevec and Zoja Vukmanovic are warmly acknowledged, along with the editorial handling of Eduardo Mansur and Bernd Lehmann. The support of the DSI-NRF Centre of Excellence (CoE) for Integrated Mineral and Energy Resource Analysis (DSI-NRF CIMERA) towards this research is hereby acknowledged. Opinions expressed and conclusions arrived at, are those of the author(s) and are not necessarily to be attributed to the CoE.

Funding Open access funding provided by University of the Witwatersrand.

Declaration

This research was funded by DSI-NRF CIMERA. One author (JV) is an employee of Impala Bafokeng. There are no further conflicts of interest to declare, as far as the first author is aware.

Reference list

Arndt N, Jenner G, Ohnenstetter M, Deloule E, Wilson AH (2005) Trace elements in the Merensky Reef and adjacent norites Bushveld Complex, South Africa, vol 40. Mineralium Deposita, pp 550–575. https://doi.org/10.1007/s00126-005-0030-x

Ballhaus C, Ryan CG (1995) Platinum-group elements in the Merensky Reef. I. PGE in solid solution in base metal sulphides and the down-temperature equilibration of Merensky ores. Contrib Miner Petrol 122:241–251. https://doi.org/10.1007/s0041000050124

Ballhaus CG, Stumpfl EF (1986) Sulphide and platinum mineralization in the Merensky reef: evidence from hydrous silicates and fluid inclusions. Contrib Miner Petrol 94:193–204. https://doi.org/10.1007/BF00592936

Ballhaus C, Sylvester P (2000) Noble metal enrichment processes in the merensky reef, bushveld complex. J Petrol 41(4):545–561 https://doi.org/10.1093/petrology/41.4.545

Barnes SJ, Campbell IH (1988) Role of late magmatic fluids in Merensky-type platinum deposits: a discussion. Geology 16(6):488–491. https://doi.org/10.1130/0091-7613(1988)016%3C0488:ROLMFI3E2.3.CO;2

Barnes Sarah-Jane, Wolfgang D Maier, Edward A Curl (2010) Composition of the marginal rocks and sills of the rustenburg layered suite, bushveld complex, South Africa: implications for the formation of the platinum-group element deposits. Econ Geol 105(8):1491–1511 https://doi.org/10.2113/econgeo.105.8.1491

Barnes Stephen J, Cruden Alexander R, Arndt Nicholas et al (2016) The mineral system approach applied to magmatic Ni–Cu–PGE sulphide deposits. Ore Geology Reviews 76:296–316 https://doi.org/10.1016/j.oregeorev.2015.06.012

Bergantz GW, Schleicher JM, Burgisser A (2015) Open-system dynamics and mixing in magma mushes. Nat Geosci 8(10):793–796. https://doi.org/10.1038/ngeo2534

Boudreau AE (1999) Fluid fluxing of cumulates: the JM reef and associated rocks of the Stillwater Complex. Mont J Petrol 40(5):755–772. https://doi.org/10.1093/petroj/40.5.755

Boudreau AE (2008) Modelling the Merensky Reef, Bushveld Complex, Republic of South Africa. Contrib Miner Petrol 156:431–437. https://doi.org/10.1007/s00410-008-0294-0

Bourdeau JE, Hayes B, Zhang SE, Logue A, Bybee GM (2022) Origin and significance of noritic blocks in layered anorthosites in the Bushveld Complex, South Africa. Contrib Miner Petrol 177(1):11. https://doi.org/10.1007/s00410-021-01872-8

Bourdeau JE, Zhang SE, Hayes B, Logue A, Bybee GM (2023) Evidence for the incremental assembly of the pyroxenite marker, Bushveld Complex, by the emplacement of crystal slurries. Lithos 438:107007. https://doi.org/10.1016/j.lithos.2022.107007

Brügmann GE, Naldrett AJ, Asif M, Lightfoot PC, Gorbachev NS, Fedorenko VA (1993) Siderophile and Chalcophile metals as tracers of the evolution of the siberian trap in the Noril'Sk region, Russia. Geochim Cosmochim Acta 57(9):2001–2018. https://doi.org/10.1016/0016-7037(93)90089-F

Cameron EN (1980) Evolution of the lower critical zone, central sector, eastern Bushveld Complex, and its chromite deposits. Econ Geol 75(6):845–871. https://doi.org/10.2113/gsecongeo.75.6.845

Campbell IH, Naldrett AJ, Barnes SJ (1983) A model for the origin of the platinum-rich sulfide horizons in the Bushveld and Stillwater Complexes. J Petrol 24(2):133–165. https://doi.org/10.1093/petrology/24.2.133

Cawthorn RG (1999) The discovery of the platiniferous Merensky reef in 1924. S Afr J Geol 102(3):178–183. https://doi.org/10.10520/EJC-112518d32d

Cawthorn RG (1999a) Permeability of the footwall cumulates to the Merensky reef, Bushveld Complex. S Afr J Geol 102(3):293–310. https://doi.org/10.10520/EJC-1125b7f876

Cawthorn RG (2015) The Bushveld Complex, South Africa. In: Charlier B, Namur O, Latypov R, Tegner C (eds) Layered intrusions. Springer Geology. Springer, Dordrecht, pp 517–587. https://doi.org/10.1007/978-94-017-9652-1_12

Cawthorn RG, Boerst K (2006) Origin of the pegmatitic pyroxenite in the Merensky unit, Bushveld Complex, South Africa. J Petrol 47(8):1509–1530. https://doi.org/10.1093/petrology/egl017

Cawthorn RG, Meyer PS, Kruger FJ (1991) Major addition of magma at the pyroxenite marker in the western Bushveld Complex, South Africa. J Petrol 32(4):739–763. https://doi.org/10.1093/petrology/32.4.739

Chutas NI, Bates E, Prevec SA, Coleman DS, Boudreau AE (2012) Sr and Pb isotopic disequilibrium between coexisting plagioclase and orthopyroxene in the Bushveld Complex, South Africa: microdrilling and progressive leaching evidence for sub-liquidus contamination within a crystal mush. Contrib Miner Petrol 163:653–668. https://doi.org/10.1007/s00410-011-0691-7

Davies G, Tredoux M (1985) The platinum-group element and gold contents of the marginal rocks and sills of the Bushveld Complex. Econ Geol 80(4):838–848. https://doi.org/10.2113/gsecongeo.80.4.838

Eales HV, Field M, de Klerk WJ, Scoon RN (1988) Regional trends of chemical variation and thermal erosion in the Upper critical zone, western Bushveld Complex. Mineral Mag 52:63–79. https://doi.org/10.1180/minmag.1988.052.364.06

Elburg MA, Cawthorn RG (2017) Source and evolution of the alkaline Pilanesberg Complex, South Africa, vol 455. Chemical Geology, pp 148–165. https://doi.org/10.1016/j.chemgeo.2016.10.007

Elburg MA, Vroon P, van der Wagt B, Tchalikian A (2005) Sr and Pb isotopic composition of give USGS glasses (BHVO-2G, BIR-1G, BCR-2G, TB-1G, NKT-1G). Chem Geol 223:196–207. https://doi.org/10.1016/j.chemgeo.2005.07.001

Ernst RE (2014) Large igneous provinces. Cambridge University Press. https://doi.org/10.1017/CBO9781139025300

Godel B, Barnes SJ, Maier WD (2007) Platinum-group elements in sulphide minerals, platinum-group minerals, and whole-rocks of the Merensky reef (Bushveld Complex, South Africa): implications for the formation of the reef. J Petrol 48(8):1569–1604. https://doi.org/10.1093/petrology/egm030

Grobler DF, Brits JAN, Maier WD, Crossingham A (2019) Litho-and chemostratigraphy of the flatreef PGE deposit, northern bushveld complex. Miner Deposita 54(1):3–28. https://doi.org/10.1007/s00126-018-0800-x

Harmer RE, Sharpe MR (1985) Field relations and strontium isotope systematics of the marginal rocks of the eastern Bushveld Complex. Econ Geol 80(4):813–837. https://doi.org/10.2113/gsecongeo.80.4.813

Hayes B, Ashwal LD, Webb SJ, Bybee GM (2017) Large-scale magmatic layering in the Main Zone of the Bushveld Complex and episodic downward magma infiltration. Contrib Miner Petrol 172:1–16. https://doi.org/10.1007/s00410-017-1334-4

Hayes B, Bybee GM, Mawela M, Nex PA, van Niekerk D (2018) Residual melt extraction and out-of-sequence differentiation in the Bushveld Complex, South Africa. J Petrol 59(12):2413–2434. https://doi.org/10.1093/petrology/egy101

Holness MB, Vukmanovic Z, Mariani E (2017) Assessing the role of compaction in the formation of adcumulates: a microstructural perspective. J Petrol 58(4):643–673. https://doi.org/10.1093/petrology/egx037

Holwell DA, McDonald I, Armitage PEB (2006) Platinum-group mineral assemblages in the platreef at the Sandsloot Mine, northern Bushveld Complex, South Africa. Mineral Mag 70(1):83–101. https://doi.org/10.1180/0026461067010315

Irvine TN (1977) Origin of chromitite layers in the muskox intrusion and other stratiform intrusions: a new interpretation. Geology 5(5):273–277 https://doi.org/10.1130/0091-7613(1977)5<273:OOCLIT>2.0.CO;2

Irvine TN, Keith DW, Todd SG (1983) The JM platinum-palladium reef of the Stillwater Complex, Montana; II, origin by double-diffusive convective magma mixing and implications for the Bushveld Complex. Econ Geol 78(7):1287–1334. https://doi.org/10.2113/gsecongeo.78.7.1287

Kaufmann FE, Vukmanovic Z, Holness MB, Hecht L (2018) Orthopyroxene oikocrysts in the MG1 chromitite layer of the Bushveld Complex: implications for cumulate formation and recrystallisation. Contrib Miner Petrol 173:1–20. https://doi.org/10.1007/s00410-018-1441-x

Kinnaird JA (2005) Geochemical evidence for multiphase emplacement in the southern Platreef. Appl Earth Sci 114(4):225–242. https://doi.org/10.1179/037174505X82152

Kinnaird JA, Yudovskaya M, McCreesh M, Huthmann F, Botha TJ (2017) The Waterberg platinum group element deposit: atypical mineralisation in mafic-ultramafic rocks of the Bushveld Complex, South Africa. Econ Geol 112(6):1367–1394. https://doi.org/10.5382/econgeo.2017.4513

Kruger FJ (1992) The origin of the Merensky cyclic unit: Sr-isotopic and mineralogical evidence for an alternative orthomagmatic model. Aust J Earth Sci 39(3):255–261. https://doi.org/10.1080/08120099208728021

Kruger FJ (2005) Filling the Bushveld Complex magma chamber: lateral expansion, roof and floor interaction, magmatic unconformities, and the formation of giant chromitite, PGE and Ti-V-magnetitite deposits. Miner Deposita 40:451–472. https://doi.org/10.1007/s00126-005-0016-8

Latypov R, Chistyakova S, Page A, Hornsey R (2015) Field evidence for the in situ crystallization of the Merensky reef. J Petrol 56(12):2341–2372. https://doi.org/10.1093/petrology/egv023

Latypov R, Chistyakova S, Barnes SJ, Hunt EJ (2017) Origin of platinum deposits in layered intrusions by in situ crystallization: evidence from undercutting Merensky reef of the Bushveld Complex. J Petrol 58(4):715–761. https://doi.org/10.1093/petrology/egx032

Latypov R, Chistyakova S, Barnes SJ, Godel B, Delaney GW, Cleary PW, Radermacher VJ, Campbell I, Jakata K (2022) Chromitite layers indicate the existence of large, long-lived, and entirely molten magma chambers. Sci Rep 12(1):4092. https://doi.org/10.1038/s41598-022-08110-6

Lauder WR (1970) Origin of the Merensky reef. Nature 227(5256):365–366. https://doi.org/10.1038/227365a0

Lee CA, Butcher AR (1990) Cyclicity in the Sr isotope stratigraphy through the Merensky and Bastard reef units, Atok Section, eastern Bushveld Complex. Econ Geol 85:877–883. https://doi.org/10.2113/gsecongeo.85.4.877

Leeb-Du Toit A (1986) The impala platinum mines. In: Anhaeusser CR, Maske S (eds) Mineral deposits of Southern Africa. Geological Society of South Africa, Johannesburg, pp 1091–1106

Maghdour-Mashhour R, Hayes B (2021) A turbulent magmatic density current and the origin of the anastomosing UG-1 chromitites at Dwars River in the Bushveld Complex. J Petrol 62(7):egab056. https://doi.org/10.1093/petrology/egab056

Maghdour-Mashhour R, Hayes B, Bolhar R, Ueckermann H (2021) Sill intrusion into pyroxenitic mush and the development of the Lower–Upper critical zone boundary of the Bushveld Complex: implications for the origin of stratiform anorthosites and chromitites in layered intrusions. J Petrol 62(1):egaa090. https://doi.org/10.1093/petrology/egaa090

Maier WD, Barnes SJ (1999) Platinum-group elements in silicate rocks of the lower, critical and main zones at Union Section, western Bushveld Complex. J Petrol 40(11):1647–1671. https://doi.org/10.1093/petroj/40.11.1647

Maier WD, Eales HV (1997) Correlation within the UG2 – merensky reef interval of the Western Bushveld Complex, based on geochemical, mineralogical and petrological data. Geol Surv South Afr Bull 120:56

Maier WD, Arndt NT, Curl EA (2000) Progressive crustal contamination of the Bushveld Complex: evidence from nd isotopic analyses of the cumulate rocks. Contrib Miner Petrol 140:316–327. https://doi.org/10.1007/s004100000186

Maier WD, Abernethy KEL, Grobler DF, Moorhead G (2021) Formation of the Flatreef deposit, northern Bushveld, by hydrodynamic and hydromagmatic processes. Miner Deposita 56:11–30. https://doi.org/10.1007/s00126-020-00987-5

Mansur ET, Barnes SJ, Duran CJ, Sluzhenikin SF (2020) Distribution of chalcophile and platinum-group elements among pyrrhotite, pentlandite, chalcopyrite and cubanite from the Noril'Sk-Talnakh ores: implications for the formation of platinum-group minerals. Miner Deposita 55:1215–1232. https://doi.org/10.1007/s00126-019-00926-z

Marsh BD (2013) On some fundamentals of igneous petrology. Contrib Miner Petrol 166:665–690. https://doi.org/10.1007/s00410-013-0892-3

Mathez EA (1995) Magmatic metasomatism and formation of the Merensky reef, Bushveld Complex. Contrib Miner Petrol 119(2–3):277–286. https://doi.org/10.1007/BF00307287

Mathez EA, Kinzler RJ (2017) Metasomatic chromitite seams in the Bushveld and Rum layered intrusions. Elements 13(6):397–402. https://doi.org/10.2138/gselements.13.6.397

Mathez EA, Hunter RH, Kinzler R (1997) Petrologic evolution of partially molten cumulate: the Atok section of the Bushveld Complex. Contrib Miner Petrol 20–34. 129https://doi.org/10.1007/s004100050320

McDonald I, Holwell DA, Armitage PE (2005) Geochemistry and mineralogy of the platreef and critical zone of the northern lobe of the Bushveld Complex, South Africa: implications for Bushveld stratigraphy and the development of PGE mineralisation. Miner Deposita 40:526–549. https://doi.org/10.1007/s00126-005-0018-6

Mitchell AA, Manthree R (2002) The Giant Mottled Anorthosite: a transitional sequence at the top of the Upper critical zone of the Bushveld Complex. S Afr J Geol 105:15–24. https://doi.org/10.2113/1050015

Mitchell AA, Scoon RN (2007) The Merensky reef at Winnaarshoek, Eastern Bushveld Complex: a primary magmatic hypothesis based on a wide reef facies. Econ Geol 102(5):971–1009. https://doi.org/10.2113/gsecongeo.102.5.971

Mitchell AA, Scoon RN, Sharpe MR (2019) The Upper critical zone in the Swartklip Sector, north-western Bushveld Complex, on the farm Wilgerspruit 2JQ: II. Origin by intrusion of ultramafic sills with concomitant partial melting of host norite-anorthosite cumulates. S Afr J Geol 122:143–162. https://doi.org/10.25131/sajg.122.0011

Moodley P (2008) Facies variation in the Merensky Reef at Bafokeng Rasimone Platinum mine. Southern African Institute of Mining and Metallurgy, Platinum in Transformation, pp 87–95

Mungall JE, Kamo SL, McQuade S (2016) U-Pb geochronology documents out-of-sequence emplacement of ultramafic layers in the Bushveld Igneous Complex of South Africa. Nat Commun 7:13385. https://doi.org/10.1038/ncomms13385

Mungall JE, Jenkins MC, Robb SJ, Yao Z, Brenan JM (2020) Upgrading of magmatic sulfides, revisited. Econ Geol 115(8):1827–1833. https://doi.org/10.5382/econgeo.4775

Naldrett AJ, Gasparrini EC, Barnes SJ, Von Gruenewaldt G, Sharpe MR (1986) The Upper critical zone of the Bushveld Complex and the origin of Merensky-type ores. Econ Geol 81(5):1105–1117. https://doi.org/10.2113/gsecongeo.81.5.1105

Naldrett AJ, von Gruenewaldt G (1989) Association of platinum-group elements with chromitite in layered intrusions and ophiolite complexes. Econ Geol 84(1):180–187 https://doi.org/10.2113/gsecongeo.84.1.180

Naldrett AJ, Wilson A, Kinnaird J, Chunnett G (2009) PGE tenor and metal ratios within and below the Merensky Reef, Bushveld Complex: implications for its genesis. J Petrol 50(4):625–659. https://doi.org/10.1093/petrology/egp015

Nex PAM, Cawthorn RG, Kinnaird JA (2002) Geochemical effects of magma addition: compositional reversals and decoupling of trends in the Main Zone of the western Bushveld Complex. Mineral Mag 66(6):833–856. https://doi.org/10.1180/0026461026660063

Nicholson DM, Mathez EA (1991) Petrogenesis of the Merensky Reef in the Rustenburg section of the Bushveld Complex. Contrib Miner Petrol 107:293–309. https://doi.org/10.1007/BF00325100

Prevec SA (2018) Igneous Rock associations 23. The Bushveld Complex, South Africa: New insights and paradigms. Geosci Can v 45:117–135. https://doi.org/10.12789/geocanj.2018.45.138

Prevec SA, Ashwal LD, Mkaza MS (2005) Mineral disequilibrium in the Merensky Reef, western Bushveld Complex, South Africa: new Sm–Nd isotopic evidence. Contrib Miner Petrol 149:306–315. https://doi.org/10.1007/s00410-005-0650-2

Prevec SA, Largatzis SA, Brownscombe W, Salge T (2021) PGE distribution in Merensky wide-reef facies of the Bushveld Complex, South Africa: evidence for localized hydromagmatic control. Can Mineral 59(6):1305–1338. https://doi.org/10.3749/canmin.2100033

Scoates JS, Wall CJ (2015) Geochronology of layered intrusions. In: Charlier B, Namur O, Latypov R, Tegner C (eds) Layered intrusions. Springer Geology. Springer, Dordrecht, pp 3–74. https://doi.org/10.1007/978-94-017-9652-1_1

Scoates JS, Wall CJ, Friedman RM, Weis D, Mathez EA, VanTongeren JA (2021) Dating the Bushveld Complex: timing of crystallization, duration of magmatism, and cooling of the world's largest layered intrusion and related rocks. J Petrol 62(2):pegaa107. https://doi.org/10.1093/petrology/egaa107

Scoon RN, Mitchell AA (2023) Petrogenesis of the Marginal Sill Phase and Lower Zone in the Eastern Limb of the Bushveld Complex: incremental development of igneous layering and syn-magmatic emplacement of peridotite intrusions and sills. S Afr J Geol 126(4):425–450. https://doi.org/10.25131/sajg.126.0021

Seabrook CL, Cawthorn RG, Kruger FJ (2005) The Merensky reef, Bushveld Complex: mixing of minerals not mixing of magmas. Econ Geol 100(6):1191–1206. https://doi.org/10.2113/gsecongeo.100.6.1191

Setera JB, VanTongeren JA (2018) Lateral variability in the Upper Main Zone, Bushveld Complex, owing to directional magma recharge and emplacement from north to south. J Petrol 59(9):1763–1786. https://doi.org/10.1093/petrology/egy081

Sharpe MR (1985) Strontium isotope evidence for preserved density stratification in the main zone of the Bushveld Complex, South Africa. Nature 316(6024):119–126. https://doi.org/10.1038/316119a0

Smith AJB, Viljoen KS, Schouwstra R, Roberts J, Schalkwyk C, Gutzmer J (2013) Geological variations in the Merensky Reef at Bafokeng Rasimone Platinum Mine and its influence on flotation performance. Miner Eng 52:155–168. https://doi.org/10.1016/j.mineng.2013.05.015

Smith W, Maier W, Barnes S, Moorhead G, Reid D, Karykowski B (2021) Element mapping the Merensky reef of the Bushveld Complex. Geosci Front 12(3):101101. https://doi.org/10.1016/j.gsf.2020.11.001

Sobolev AV, Hofmann AW, Kuzmin DV, Yaxley GM, Arndt NT, Chung SL, Danyushevsky LV, Elliott T, Frey FA, Garcia MO, Gurenko AA (2007) The amount of recycled crust in sources of mantle-derived melts. Science 316(5823):412–417. https://doi.org/10.1126/science.1138113

Vermaak CF (1976) The Merensky reef; thoughts on its environment and genesis. Econ Geol 71(7):1270–1298. https://doi.org/10.2113/gsecongeo.71.7.1270

Vermeulen GJ (2010) Merensky reef Facies Delineation on the Farms Boschkoppie and Styldrift in the western Bushveld Complex. Unpublished internal report, Royal Bafokeng Resources

Viljoen MJ (1999) The nature and origin of the Merensky reef of the western Bushveld Complex based on geological facies and geophysical data. S Afr J Geol 102:221–239

Viljoen MJ, De Klerk WJ, Coetzer PM, Hatch NP, Kinloch E, Peyerl W (1986a) The Union Section of Rustenburg Platinum Mines Limited, with reference to the Merensky Reef. In: C.R. Anhaeusser and S. Maske (Editors), Mineral Deposits of southern Africa, Volume 2, Geological Society of South Africa, Johannesburg. 1061–1090. https://cir.nii.ac.jp/crid/1571698601335131008

Wilson AH (2012) A chill sequence to the Bushveld Complex: insight into the first stage of emplacement and implications for the parental magmas. J Petrol 53(6):1123–1168. https://doi.org/10.1093/petrology/egs011

Wilson A, Chunnett G (2006) Trace element and platinum group element distributions and the genesis of the Merensky reef, Western Bushveld Complex, South Africa. J Petrol 47(12):2369–2403. https://doi.org/10.1093/petrology/egl048

Wilson AH, Lee CA, Brown RT (1999) Geochemistry of the Merensky reef, Rustenburg Section, Bushveld Complex: controls on the silicate framework and distribution of trace elements. Miner Deposita 34:657–672. https://doi.org/10.1007/s001260050226

Yao Z, Mungall JE, Jenkins MC (2021) The Rustenburg Layered suite formed as a stack of mush with transient magma chambers. Nat Commun 12(1):505. https://doi.org/10.1038/s41467-020-20778-w

Yudovskaya MA, Kinnaird JA, Sobolev AV, Kuzmin DV, McDonald I, Wilson AH (2013) Petrogenesis of the Lower Zone olivine-rich cumulates beneath the platreef and their correlation with recognized occurrences in the Bushveld Complex. Econ Geol 108(8):1923–1952. https://doi.org/10.2113/econgeo.108.8.1923

Yudovskaya MA, Kinnaird JA, Costin G, McCreesh M, Shilovskikh V, Kovalchuk E, Kuzmin D (2022) Formation of spinel-orthopyroxene symplectites by reactive melt flow: examples from the northern Bushveld Complex and implications for mineralization in layered intrusions. Econ Geol 117(8):1935–1960. https://doi.org/10.5382/econgeo.4938

Zeh A, Ovtcharova M, Wilson AH, Schaltegger U (2015) The Bushveld Complex was emplaced and cooled in less than one million years – results of zirconology, and geotectonic implications. Earth Planet Sci Lett 418:103–114. https://doi.org/10.1016/j.epsl.2015.02.035

Zellmer GF, Sakamoto N, Matsuda N, Iizuka Y, Moebis A, Yurimoto H (2016) On progress and rate of the peritectic reaction fo + SiO2→ En in natural andesitic arc magmas. Geochim Cosmochim Acta 185:383–393. https://doi.org/10.1016/j.gca.2016.01.005